nature communications

Article

https://doi.org/10.1038/s41467-025-59977-8

Neoantigen enriched biomimetic nanovaccine for personalized cancer immunotherapy

Received: 3 February 2025

Accepted: 9 May 2025

Published online: 23 May 2025

Check for updates

Yuwei Li[1,2,4], Maoxin Fang[1,4], Haotian Yu[1], Xianglei Wang[1], Shiyao Xue[1], Zeze Jiang[1], Zixuan Huang[1], Shaoqin Rong[1], Xiaoli Wei[3], Zhigang Lu[2] & Min Luo[1]

Personalized cancer vaccines elicit robust T cell immunity and anti-tumour potency, but identifying tumour-specific antigens remains challenging, severely constraining the therapeutic window. Biomimetic nanovaccines employing cancer cell membranes display inherent biocompatibility and stimulate T-cell responses against diverse tumour antigens, though tumours develop multiple mechanisms to reduce antigen presentation. Here we demonstrate a rapid and general strategy to fabricate personalized nanovaccines based on Antigen-Enriched tumor Cell Membranes (AECM) for early intervention. Interferon-γ potently stimulates antigen presentation across a broad range of cancer cell types. By coupling the generated AECM with PC7A adjuvant, a stimulator of interferon genes (STING)-activating polymer, the AECM@PC7A nanovaccine induces robust poly-neoepitopic T-cell responses even at low dosage, achieving significant tumour regression and metastasis inhibition in multiple murine cancer models. This anti-tumor response relies on MHC-I restricted antigen presentation and $CD8^+$ T-cell activation, with dendritic cells presenting AECM antigens predominantly via cross-dressing to prime T-cells. AECM@PC7A exhibits remarkable anti-tumor efficacy when compared to vaccines with diverse formulations, and demonstrates therapeutic potential in post-surgical and humanized xenograft tumor models. This proof-of-concept study provides a promising universal avenue for the rapid development of personalized cancer vaccines applicable to early intervention for a broad range of patients.

Immune checkpoint blockade and CAR-T therapy have shown the central roles of T-cell immunity in cancer immunotherapy[1]. Therapeutic cancer vaccines, including nanovaccines, can induce potent anti-tumour T-cell response through delivering tumour antigens together with immune adjuvants[2–5]. Tumour neoantigens derived from somatic mutations are exclusively expressed by tumour cells[6,7], providing the opportunity to circumvent T-cell central tolerance of self-epitopes and thus induce tumour-specific T cell response for cancer eradication[8]. Multiple approaches have been developed to improve neoantigens predication and verification[9,10]. Personalised neoantigen

[1]Institute of Pediatrics of Children's Hospital of Fudan University, the Shanghai Key Laboratory of Medical Epigenetics, the International Co-laboratory of Medical Epigenetics and Metabolism, Ministry of Science and Technology, Institutes of Biomedical Sciences, Fudan University, Shanghai, China. [2]The Fifth People's Hospital of Shanghai, Institutes of Biomedical Sciences, Fudan University, Shanghai, China. [3]Department of Pharmacology, School of Basic Medical Sciences, Fudan University, Shanghai, China. [4]These authors contributed equally: Yuwei Li, Maoxin Fang. e-mail: luo_min@fudan.edu.cn

vaccines, with high immunogenicity and tumour specificity, are being tested in clinical trials and have shown promising outcome[3,11–14]. However, the efficiency of neoantigen discovery remains low currently, with <6% prediction positive rate[11,15]. In particularly, the entire vaccine developing procedure is time-consuming, usually requiring ~3 months for one round of screening and preparation[10,13]. Thus, the therapeutic window is considerably restricted, and many cancer patients miss early intervention, severely limiting the widespread application of neoantigen-based vaccines in clinical practice. Strategy to design personalised cancer vaccine in a fast and effective way is required.

Biomimetic cancer vaccines using autologous cell-derived components have gained extensive attention in personalised immunotherapy[16–19]. Cancer cells can afford a wide range of tumour antigens from patients, allowing poly-epitopic cytotoxic T lymphocyte (CTL) responses without the need for precise antigen identification and synthesis. Clinical trials of vaccines using cancer cell lysates (e.g., Melacine) or irradiated whole cancer cells (such as GVAX, Canvaxin, STINGVAX) have been undergoing in melanoma, breast, pancreatic, colorectal, and prostate cancer patients[20–23]. Notably, cancer cell membranes harbour tumour antigens that have already undergone MHC/HLA processing[24], offering advantages in triggering tumour-specific T-cell responses. Recently, diverse cancer cells have been explored in the formulations of cell membrane-based nanovaccines to further accelerate the stimulation of various T cells. These vaccines are capable of inducing effective anti-tumour responses in vivo and synergise well with other immunotherapies, such as checkpoint blockades[25–30].

Nevertheless, tumours develop multiple mechanisms to diminish the antigen presentation, such as antigen depletion and reduced surface expression of HLA-I/MHC-I through modulation of transcription and genetic alterations[24,31–33]. Consequently, high dosage of cancer-cell-based vaccines is usually required to elicit tumour-specific T cell response, posing challenges to sample collection and potentially increasing side effects[29,34]. Therefore, increasing tumour specific antigen abundance and immunogenicity on cancer cells by therapeutic agents and using the membranes of these cells as the antigen source would provide opportunities to overcome these limitations to prompt the clinical use of personalised cancer vaccines.

We previously developed a STING-activating nanovaccine by a straightforward mixing of antigen peptides with a synthetic polymer, PC7A, eliciting robust anti-tumour T-cell response in multiple tumour models[35–37]. Besides of facilitating peptide delivery and cytosolic release, PC7A is a polyvalent STING agonist, serving as a strong vaccine adjuvant to activate innate immune responses[35,36]. PC7A has presented an optimal safety evaluation in rats and cynomolgus monkeys[38] and is presently undergoing Phase I clinical trial (NCT06022029) for solid cancer treatment.

In this study, we perform a high-throughput analysis and revealed IFN-γ as a potent stimulator for antigen presentation across diverse cancer cell types. The Antigen-Enriched Cell Membrane coated PC7A nanovaccine (AECM@PC7A) induces robust poly-epitopic T-cell responses, leading to potent anti-tumour efficacies in diverse murine cancer models and the humanised xenograft model, presenting a universal platform for personalised cancer vaccine design in a simple and effective way.

Results

Antigen enrichment on cell membranes by IFN-γ stimulation

We first sought to obtain a therapeutic stimulator that can induce potent antigen presentation on different type of cancer cells. Antigen presentation is regulated by multiple pathways, such as those of IFN-γ, NF-κB, MEK and EGFR, and the related molecules have been reported to stimulate antigen expression in different settings[39–42]. We thus treated B16-OVA melanoma cells with a library containing 1738 FDA approved drugs and 50 cytokines/chemokines, in which the 7 known MHC-I stimulators were involved. Ten molecules were found to increase MHC-I levels by at least 3-100 folds, including the known IFN-γ and TNF-α (Fig. 1a and Supplementary Dataset.1). Notably, among these stimulators, IFN-γ, a pleiotropic cytokine that plays important roles in MHC/HLA presentation[43], and subsequently Idarubicin, an inhibitor of DNA topoisomerase II, exhibited the most robust MHC-I stimulation and minimal cytotoxicity across the six murine cancer cell lines (Fig. 1b, c, and Supplementary Dataset.2). OVA presentation on B16-OVA cells was then assessed using the antibody 25-D1.16 which recognises H2-kb-SIINFEKEL complex. Results showed that IFN-γ stimulates the highest OVA presentation, increasing by ~8.5-fold compared to control, while maintaining low cytotoxicity (Fig. 1d, e, and Supplementary Table.1).

We then assessed the broadness of IFN-γ in stimulating HLA-I presentation by analyzing 27 human tumour cell lines from 17 malignancies. Consistent with the literature, surface levels of HLA-I on most human cancer cell lines were low[32]. Following IFN-γ treatment, the HLA-I expression increased in 23 out of 27 human cell lines by 2–12 folds (Fig. 1f, and Supplementary Table.2). Thus, IFN-γ was a potent stimulator of HLA-I/MHC-I expression in a broad range of cancer cell types.

To determine if IFN-γ enhanced antigen presentation could stimulate a stronger T-cell response, we isolated cell membranes (CMs) from B16-OVA cells with or without IFN-γ treatment. CMs exhibited a high abundance of Na^+/K^+-ATPase, a marker of membranes (Supplementary Fig. 1a). The protein levels of MHC-I and H2-kb-OVA in CMs from IFN-γ treated cells (Antigen Enriched Cell Membrane, AECM) was significantly higher than control (Fig. 1g, h), consistent with their expression pattern on cell surface. When co-incubated with the OT-I T-cells, AECM stimulated OVA-specific $CD8^+$ T-cell proliferation ~10-folds more than control CM, and significantly increased the proportion of activated T-cells ($CD69^+$) (CM, 18.7%; AECM, 44.3%) (Fig. 1i, j). Notably, the AECM activates OT-I T-cell proliferation in a dose-dependent manner (Fig. 1k, l). Thus, AECM contained enriched immunogenic antigens to stimulate antigen specific $CD8^+$ T-cell response, suggesting its potential as a suitable source of tumour antigens for cancer vaccine.

AECM@PC7A stimulates APC maturation and T cell priming

We then generated Antigen Enriched Cell Membrane coated PC7A nanovaccine (AECM@PC7A) by mixing AECM with PC7A at a ratio of 10:3 followed by sonication[28,44]. CM@PC7A using non-treated CM was also generated for comparison. In this formulation, PC7A, exhibiting a strong vaccine adjuvant effect via a direct activation of STING[35,36], served as an adjuvant, as well as a carrier of free antigens potentially released from membranes during sonication. The nanoparticles showed an average hydrodynamic diameter of ~120 nm, with comparable zeta potentials (−22.68 ±0.24 mV) to that of cell membranes (−23.45±0.46 mV) (Supplementary Fig. 1b, c), suggesting the successful coating of cell membrane around PC7A. Additionally, these particles retained the membrane lysing ability of PC7A at pH below 7.0 (Supplementary Fig. 1d, e), which will facilitate cytosol release of antigens when uptake by DCs into endosomes[35,45].

The potency of AECM@PC7A to induce APC maturation and antigen-specific T-cell priming was assessed (Fig. 2a). Bone marrow derived dendritic cells (BMDCs) were treated with CMs or CMs-derived PC7A nanovaccines from B16-OVA cells for 1 day, and then harvested to evaluate their T-cell priming activity by coculture with OT-I splenocytes. Consistent with its roles as an adjuvant[35,36], PC7A was able to induce BMDCs maturation either alone or in the forms of nanovaccine, achieving higher expression of CD80 and CD86 than those without PC7A (Fig.2b). BMDCs treated with either control CM or CM@PC7A cannot stimulate OT-I $CD8^+$ T-cell proliferation until its concentration was increased up to 200μg/mL, confirming the low OVA-antigen presence on these untreated cell membranes (Fig. 2c, d,

https://doi.org/10.1038/s41467-025-59977-8

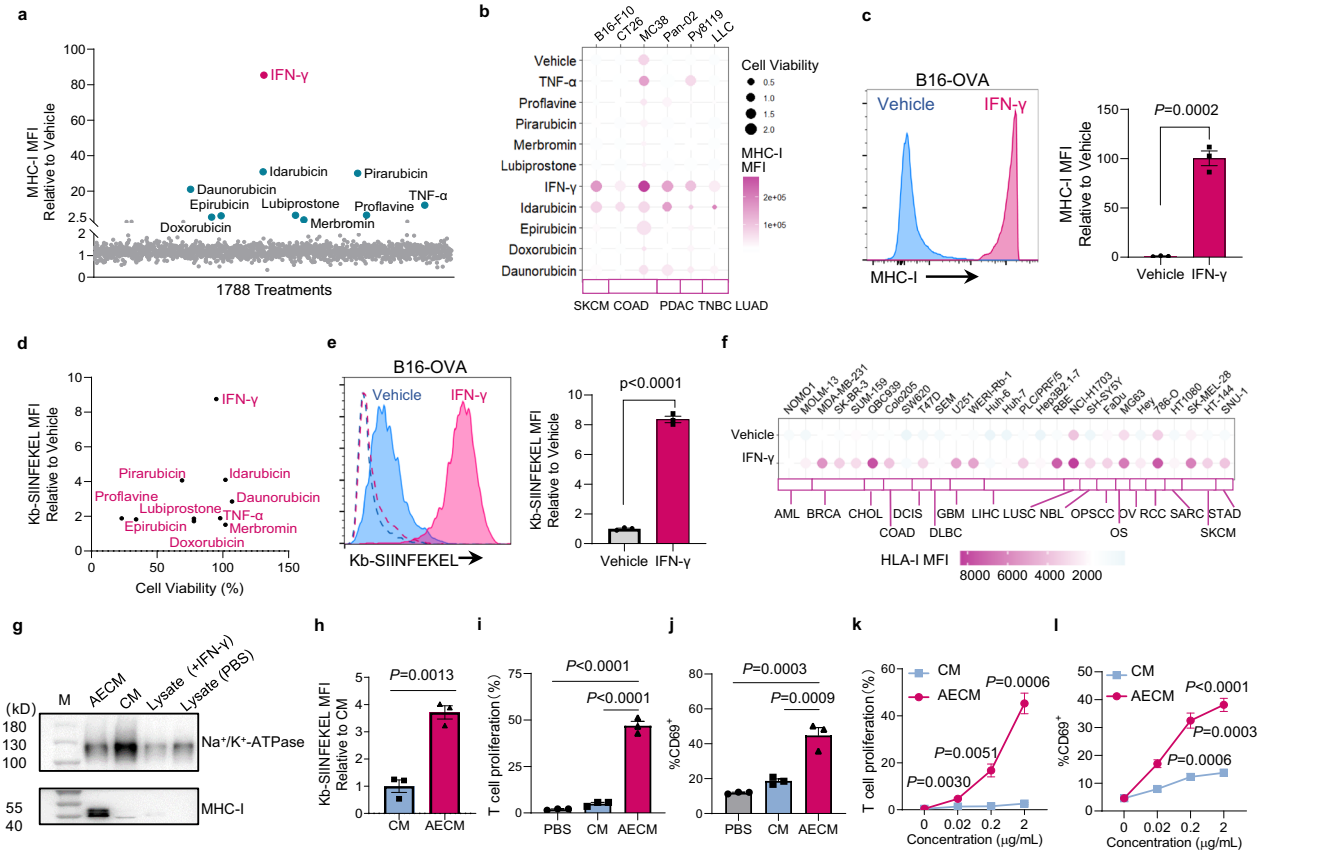

Fig. 1 | Enhanced antigen presentation on the membrane of IFN-γ-stimulated cancer cells. a MHC-I surface expression on B16-OVA cells post 1788 treatments. **b** MHC-I surface expression on indicated murine cell lines and the cell viabilities relative to control by different treatments. SKCM Skin Cutaneous Melanoma, COAD Colorectal Adenocarcinoma, PDAC Pancreatic Ductal Adenocarcinoma, TNBC Triple-Negative Breast Cancer, LUAD Lung Adenocarcinoma. **c** Representative FACS histograms and quantification of MHC-I expression on B16-OVA cells with or without IFN-γ treatment (n = 3 independent experiments). **d** OVA presentation on B16-OVA cells and cell viabilities by different treatments. **e** Representative FACS histograms and quantification showing OVA-presentation on IFN-γ treated and control B16-OVA cells. Dashed lines, isotype; solid lines, anti-Kb-SIINFEKEL. (n = 3 independent experiments). **f** HLA-I surface levels on indicated human cell lines with or without IFN-γ treatment. AML Acute Myeloid Leukemia, BRCA Breast Cancer, CHOL Cholangiocarcinoma, DCIS Ductal Carcinoma in Situ, GBM Glioblastoma Multiforme, LIHC Liver Hepatocellular Carcinoma, LUSC Lung Squamous Cell Carcinoma, NBL Neuroblastoma, OPSCC Oropharyngeal Squamous Cell Carcinoma, OV Ovarian Cancer, RCC Renal Cell Carcinoma, SARC Sarcoma, STAD Stomach Adenocarcinoma, DLBC Diffuse Large B-Cell Lymphoma, OS Osteosarcoma. **g** Western blot showing Na^+/K^+-ATPase and MHC-I in the cell membranes and cell lysates of B16-OVA cells with or without IFN-γ treatment. **h** OVA-presentation on AECMs or CMs of B16-OVA cells as determined by flow cytometry. OT-I T-cells were incubated with 2 μg/mL B16-OVA derived CM or AECM for 48 days, T-cell proliferation rate (**i**) and CD69 expression (**j**) in $CD8^+$ T-cells were shown (n = 3 independent experiments). OT-I T-cells were incubated with B16-OVA derived CM or AECM for 3 days, T-cell proliferation rate (**k**) and CD69 expression (**l**) in $CD8^+$ T-cells were shown (n = 3 independent experiments). In (**c**, **e**, **h**–**l**), representative data from three independent experiments are presented as means ± s.e.m. Statistical significance was calculated by ordinary one-way ANOVA (**i**, **j**) and Student's two-sided unpaired *t*-test (**c** right, **e** right, **h**, **k**, **l**). Source data are provided as a Source Data file.

and Supplementary Fig. 2a, b). On the other hand, BMDCs treated with AECM exhibit obvious OT-I T-cell priming activity even at a low concentration of 20 μg/mL, which was further increased significantly when it was packed into AECM@PC7A (Fig. 2c, d). We had also used the purified OT-I T-cells instead of whole splenocytes for T-cell priming assay and obtained similar results (Supplementary Fig. 2c, d). Thus, these results indicates that AECM@PC7A can efficiently induce APC maturation and T-cell priming in vitro.

For further validation in vivo, we vaccinated the wildtype C57BL/6 mice three times with these B16-OVA nanovaccines at a dose of 300 μg per shot, and APC maturation and OVA-specific $CD8^+$ T-cell response were determined at day 7 after the last vaccination (Fig. 2e). Consistent with in vitro data, DCs isolated from the lymph nodes of both AECM@PC7A and CM@PC7A vaccinated mice were more mature than that of control mice, with higher proportion of $CD80^+CD86^+$ cells (Fig. 2f, g), while the expression of CD80 and CD86 in macrophages showed little difference (Supplementary Fig. 2e, f). In peripheral blood mononuclear cells (PBMCs), the percentage of $tetramer^+$ $CD8^+$ T-cells is ~7-fold and ~11-fold higher in AECM@PC7A treated mice when compared to CM@PC7A treated and control mice, respectively (Fig. 2h, i). Furthermore, when restimulated with the $OVA_{257–264}$ peptide, the $CD8^+$ T-cells from AECM@PC7A vaccinated mice produced the highest amount of IFN-γ among all groups (Fig. 2j, k). To ascertain the major APC subsets, we utilised *Batf3*$^{-/-}$ mice for cDC1s depletion or administration of clodronate liposomes to deplete macrophages. Consistent with the APC maturation data, AECM@PC7A induced T-cell response was substantially diminished in *Batf3*$^{-/-}$ mice, whereas unaffected in clodronate liposomes treated mice (Fig. 2l, m), indicating the central role of DCs to present AECM antigens. Collectively, these results demonstrated the high potency of AECM@PC7A to induce DC maturation and antigen-specific T cell priming both in vitro and in vivo.

Tumour prevention and suppression by AECM@PC7A

The prophylactic protection effect of AECM@PC7A against tumour was initially examined. Mice were subcutaneously (S.C.) vaccinated three times with 100μg nanovaccine per injection at a 5-day interval, subsequent to B16-OVA inoculation at 5 days after the final vaccination. AECM@PC7A vaccination completely protected mice from tumour

https://doi.org/10.1038/s41467-025-59977-8

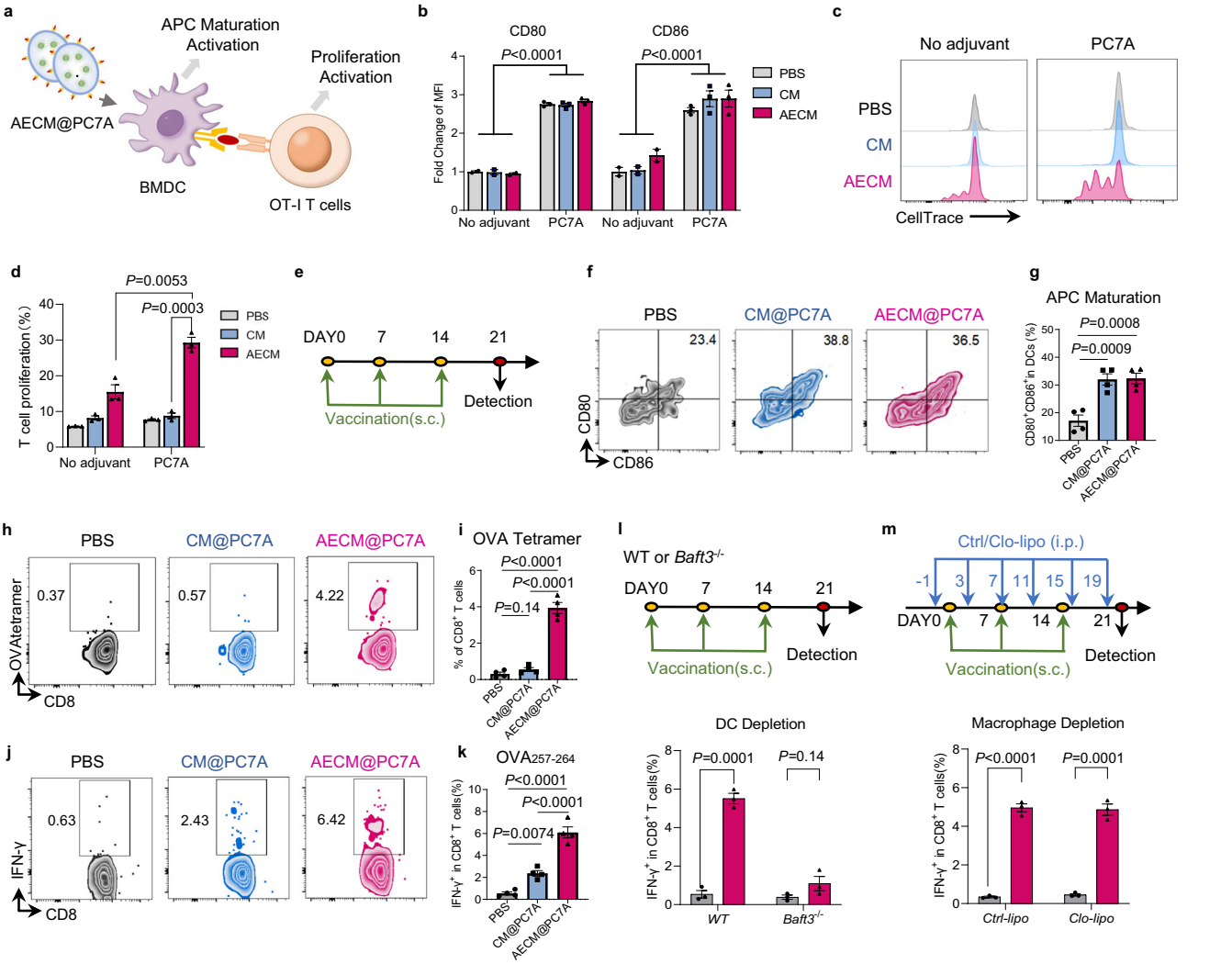

Fig. 2 | AECM@PC7A stimulates APC maturation and T-cell priming in vitro and in vivo. a–d Scheme showing determination of APC maturation and T-cell priming in vitro (**a**). BMDCs were treated with CMs or CMs-derived nanovaccines at a final concentration of 20 μg/mL for 18 h, expression of CD80 and CD86 on BMDCs were evaluated by flow cytometry (**b**, n = 2 independent experiments for No adjuvant groups, n = 3 independent experiments for PC7A groups). The treated BMDCs were harvested and co-cultured with CellTrace™ Violet-labelled OT-I splenocytes for 48 h, $CD8^+$ T-cell proliferation was shown by representative FACS histograms (**c**) and quantification (**d**, n = 3 independent experiments/group). **e–k** Vaccination timeline in mice (**e**). C57BL/6 mice received s.c. vaccinations on days 0, 7 and 14, and peripheral blood and lymph nodes were collected at day-21 for analysis. Representative scatter plots (**f**) and quantification (**g**, n = 4 mice/group) showing CD86 and CD80 expression on DCs from lymph nodes. Representative scatter plots (**h**) and quantification (**i**, n = 4 mice/group) showing OVA tetramer$^+$ $CD8^+$ cells in PBMCs. Representative scatter plots (**j**) and quantification (**k**, n = 4 mice/group) showing IFN-γ producing $CD8^+$ cells in PBMCs upon $OVA_{257-264}$-peptide restimulation. **l**, WT or *Baft3*$^{-/-}$ mice were s.c. vaccinated with AECM@PC7A three times at a dose of 300 μg per shot, PBMCs were collected at day-21 and re-stimulated with $OVA_{257-264}$ peptide, the IFN-γ secretion in $CD8^+$ T-cells were determined by ICS (n = 3 mice/group). **m** C57BL/6 mice received AECM@PC7A or PBS s.c vaccinations together with Clodronate- or control- liposomes i.p. treatment as indicated, PBMCs were collected at day-21 and re-stimulated with $OVA_{257-264}$ peptide, the IFN-γ secretion by $CD8^+$ T-cells were determined by ICS (n = 3 mice/group). In (**b**, **d**, **g**, **i**, **k**–**m**), representative data from three independent experiments are presented as means ± s.e.m. Statistical significance was calculated by ordinary one-way ANOVA (**b**, **d**, **g**, **I**, **k**) and Student's two-sided unpaired *t*-test (**l**, **m**). Source data are provided as a Source Data file. $^*P < 0.05$, $^{**}P < 0.01$, $^{***}P < 0.001$, $^{****}P < 0.0001$. NS, not significant. Source data are provided as a Source Data file.

challenge, whereas CM@PC7A showed minimal suppression on tumour growth when compared to control (Supplementary Fig. 3a). In parallel, AECM vaccines that formulated with other prevalent adjuvants, including poly I:C and colloidal manganese salt (Mn jelly, a nano-sized STING agonist[46]), were also employed for comparison. Although they also showed considerable protection, the efficacies were significantly lower than that of AECM@PC7A (Supplementary Fig. 3b), consistent with our previous findings about the superior anti-tumour activity of PC7A-OVAp vaccine over those with adjuvant of poly I:C or CpG[35].

To further evaluate the anti-tumour efficacy in established tumours, we vaccinated B16-OVA tumour-bearing mice at day 5 post-tumour inoculation when the tumour size reaches 50–100 mm^3, and followed by two booster shots with a 5-day interval. Given our prior findings that intratumoural (I.T.) injection of PC7A-OVAp triggers a positive feedback loop between myeloid-CXCL9 and T-cell-IFNγ to promote T-cell recruitment, leading to enhanced anti-tumour T-cell response compared to S.C. injection[37], we therefore compared these two routes for the administration of AECM@PC7A. Consistently, I.T. injection yielded a significantly higher potency over S.C. injection, although both effectively suppressed tumour growth (Supplementary Fig. 3c). The efficacies of AECM@ and CM@ PC7A vaccines were subsequently compared under I.T. injection. As shown in Fig. 3a–c and Supplementary Fig. 4a, tumour growths in CM@PC7A treated mice and in control mice were comparable, with all animals dying within 27 days, whereas the tumour growth was significantly inhibited by

https://doi.org/10.1038/s41467-025-59977-8

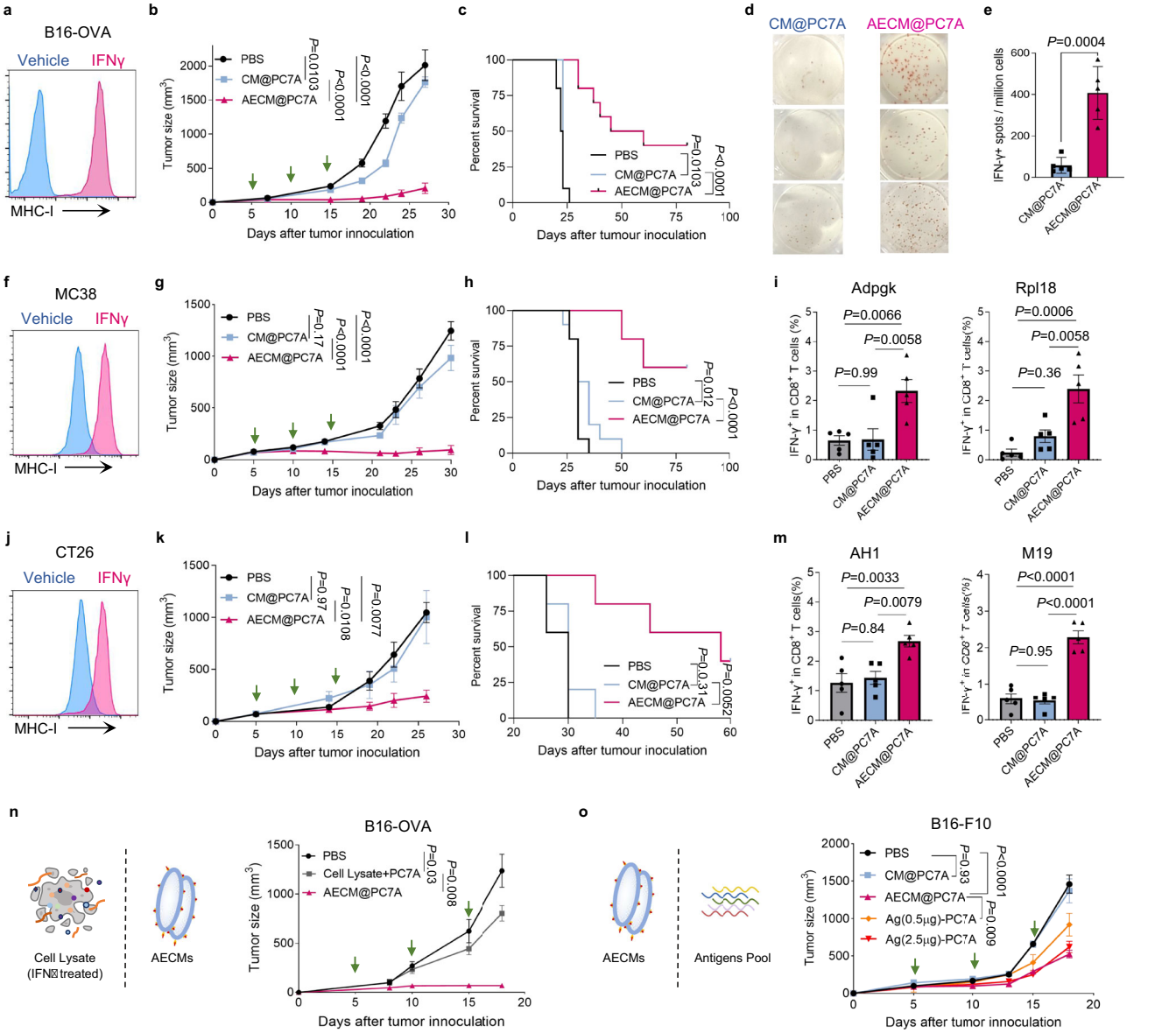

Fig. 3 | Anti-tumour efficacies of AECM@PC7A in multiple tumour models. **a** Representative histogram of MHC-I presentation on B16-OVA cells post IFN-γ treatment. **b**–**e** C57BL/6 mice inoculated with 1.5×10^5 B16-OVA cells were vaccinated at the dose of 300 μg per shot, tumour growth curves (**b**) and mice survival (**c**) were shown (n = 10 mice/group). Representative images (**d**) and quantification (**e**) of IFN-γ$^+$ ELISPOT responses in splenocytes upon re-stimulation with the $OVA_{257\text{-}264}$ peptide (n = 5 mice/group). **f** Representative histogram of MHC-I presentation on MC38 cells post IFN-γ treatment. **g**–**i** C57BL/6 mice inoculated with 2.5×10^5 MC38 cells were vaccinated at the dose of 100 μg per shot, tumour growth curves (**g**) and mice survival (**h**) were shown (n = 10 mice/group). The IFN-γ secretion by CD8$^+$ T-cells in splenocytes upon re-stimulation with Adpgk and Rpl18 neo-peptides were determined by intracellular staining (ICS) (**i**, n = 5 mice/group). **j** Representative histogram of MHC-I presentation on CT26 cells post IFN-γ treatment. **k**–**m** BALB/c mice inoculated with 1.5×10^5 CT26 cells were vaccinated at the dose of 300 μg per shot, tumour growth curves (**k**) and mice survival (**l**) were shown (n = 5 mice/group). The IFN-γ secretion by CD8$^+$ T-cells in splenocytes upon re-stimulation with AH1 or M19 neo-peptides was determined by ICS (**m**, n = 5 mice/group). **n** C57BL/6 mice inoculated with 1.5×10^5 B16-OVA cells were treated three doses of PC7A vaccines that incorporated 300 μg AECM or cell lysates from IFN-γ treated B16-OVA cells, tumour growth curves were shown (n = 5 mice/group). **o**, C57BL/6 mice inoculated with 1.5×10^5 B16-F10 cells were treated three doses of PC7A vaccines that incorporated 500 μg AECM/CM of B16-F10, or 0.5 μg/2.5 μg peptide pool (with equivalent ratio of $Gp100_{21\text{–}41}$, $Trp1_{214\text{–}237}$, $Trp2_{173\text{–}196}$, B16-M27, B16-M33), tumour growth curves were shown (n = 5 mice/group). In (**b**, **g**, **k**, **n**, **o**) representative data from three independent experiments are presented as means ± s.e.m. Statistical significance was calculated by ordinary one-way ANOVA (**b**, **g**, **i**, **k**, **m**, **n**, **o**), log-rank test (**c**, **h**, **l**) and Student's two-sided unpaired *t*-test (**e**). *$P < 0.05$, **$P < 0.01$, ***$P < 0.001$, ****$P < 0.0001$. NS not significant. Source data are provided as a Source Data file.

AECM@PC7A vaccination, with 4 out of 10 animals achieving tumour-free survival over 80 days. Enzyme-linked immunospot (ELISpot) was performed to measure the OVA-specific T-cells among splenocytes. Consistently, the number of IFN-γ-producing T-cells increased by 6.28-folds by AECM@PC7A vaccination compared to that of CM@PC7A (Fig. 3d, e). Moreover, when the splenocytes were re-stimulated with the reported neopeptides, B16-M27 and B16-M33[47], CD8$^+$ T-cells from AECM@PC7A group also produced markedly higher IFN-γ than that of CM@PC7A group (Supplementary Fig. 4b). Tumour microenvironment (TME) analysis showed that both @PC7A vaccinations resulted in higher immune cell infiltration than control treatment, consistent with the adjuvant effects of PC7A (Supplementary Fig. 4c, d). Additionally, the TME of AECM@ PC7A vaccinated mice exhibited more inflammatory when compared to CM@PC7A mice, with significantly increased anti-tumour immune cell populations, including CD8$^+$ T-cells, CD4$^+$ T-cells and CD11c$^+$ DCs, and reduced immune-suppressive M2 tumour

associated macrophages (TAMs) (Supplementary Fig. 4d). Thus, AECM@PC7A nanovaccine was capable of eliciting efficient poly-epitopic T-cell response against B16-OVA tumours.

Anti-tumour efficacy of AECM@PC7A in multiple tumour models

Neoantigens caused by tumour-specific somatic alterations are promising therapeutic targets. To further determine whether the AECM@PC7A strategy could be applied to elicit neoantigen-specific T-cell response, MC38 and CT26 murine colon cancer cells that without exogenous OVA were selected due to their well-characterised MHC-I restricted immunogenic neoantigens Adpgk & Rpl18 and AH1 & M19, respectively[47,48].

We first investigated MC38. The basal level of surface MHC-I on MC38 was at middle-high, IFN-γ treatment increased it by ~4.5-fold (Figs. 1b, 3f, and Supplementary Dataset.2). We extracted these cell membranes to generate CM@PC7A and AECM@PC7A vaccines and evaluate their anti-tumour efficacies in MC38 tumour-bearing mice. Both CM@PC7A and AECM@PC7A administrated at 300μg per shot significantly inhibited tumour growth (Supplementary Fig. 5a), consistent with the high sensitivity of MC38 to immunotherapy[49]. When decreased to 100 μg per shot, AECM@PC7A retained the high anti-tumour efficacy, with 92.3% of tumour growth inhibition compared to control and 60% of complete remission, whereas CM@PC7A treatment achieved minimal effects (Fig. 3g, h and Supplementary Fig. 5b). Moreover, the numbers of IFN-γ-producing $CD8^+$ T-cells in splenocytes upon restimulation with Adpgk and Rpl18 peptides were ~3.5-fold and ~10-fold higher, respectively, in AECM@PC7A group than those from control group, whereas no significant difference was observed between the control and CM@PC7A groups, demonstrating the high potency of AECM@PC7A to induce strong poly-neo-epitopic $CD8^+$ T-cell responses (Fig. 3i). Consistently, TME of AECM@PC7A vaccinated mice displayed a more profound anti-tumour phenotype, with significantly higher proportions of $CD8^+$ T- and $CD4^+$ T-cells and lower proportion of M2 TAMs when compared to CM@PC7A and control treated mice (Supplementary Fig. 5c).

We obtained similar results with the CT26 model. AECM@PC7A nanovaccine of CT26 stimulated robust $CD8^+$ T-cell responses against AH1 and M19 neoantigens, resulting in a more inflammatory TME and a substantial inhibition on tumour growth (Fig. 3j–m and Supplementary Fig. 6).

To further assess the efficacy of AECM vaccine, we compared its potency with that of cancer cell lysate, which also contains a full spectrum of tumour's own antigens and has shown promising outcomes[50]. As illustrated in Fig. 3n, AECM@PC7A of B16-OVA suppresses tumour growth more potently than the PC7A vaccine incorporating identical amounts of lysates of IFN-γ treated B16-OVA cells. Moreover, we also utilised the more aggressive B16-F10 tumour model to evaluate AECM vaccine and the peptide-based vaccine. For a relatively close comparison in terms of antigen diversity, five characterised antigen peptides of B16-F10 were chosen as a pool, including neoantigens (B16-M27, B16-M33) and TAAs ($Gp100_{21–41}$, $Trp1_{214–237}$, $Trp2_{173–196}$)[47]. 500 μg AECM that was generated from ~1×10^7 cells were employed for each dose. Given a normal cell harbouring ~200,000 HLA complexes on its surface[51,52], the cell membranes from 1×10^7 normal cells would potentially possess an estimated 5.5 ng of HLA-bound peptides with a presumed average length of 15 amino acids, regardless of HLA subtypes and membrane extraction efficiency. As shown in Fig. 3o, CM@PC7A exhibited little effects, whereas AECM@PC7A profoundly suppressed B16-F10 tumour growth to a level that was not attained by PC7A vaccine with pooled peptides until the dose escalated to 2.5 μg, suggesting that AECM vaccine would be more effective in stimulating anti-tumour response than that of pure antigen peptides.

Collectively, AECM@PC7A is capable of stimulating strong poly-epitopic T-cell response in multiple tumour models, achieving remarkable anti-tumour efficacy when compared to the vaccines derived from untreated cancer cell membrane, cancer cell lysate, and tumour associated antigen/neoantigen peptides.

Necessity of pMHC-I on AECM for cross-dressing to prime T-cells

We then investigate which class of MHC presented antigens is responsible to the anti-tumour effect of AECM vaccines. IFN-γ stimulates robust MHC-I upregulation but displays limited effect on MHC-II among the tested cancer cells (Supplementary Fig. 7a), suggesting the importance of MHC-I in AECM. We thus knocked out B2m, a subunit of MHC-I, in B16-OVA cells to obtain MHC-I-deficient cancer cells. MHC-I was absent in $B2m^{-/-}$ cells, while MHC-II was not affected (Fig. 4a and Supplementary Fig. 7b, c). IFN-γ did not stimulate OVA presentation on $B2m^{-/-}$ B16-OVA cells (Supplementary Fig. 7d). Consistently, the AECM from these $B2m^{-/-}$ cells was unable to activate OVA-specific $CD8^+$ T-cells when co-incubated with OT-1 splenocytes (Fig. 4b). Contrary to AECM@PC7A from WT cells, no tumour suppression was observed by B2m KO AECM@PC7A vaccination, nor was the OVA-specific $CD8^+$ T-cell activation or TME improvement (Fig. 4c–e and Supplementary Fig. 7e). For further validation, we also knocked out B2m in MC38 cells to deplete MHC-I (Fig. 4f and Supplementary Fig. 7f), and found that the B2m KO AECM@PC7A also failed to trigger tumour specific T-cell responses to suppress MC38 tumour growth (Fig. 4g–j and Supplementary Fig. 7g), indicating the requirement of MHC-I to enrich tumour responsive antigens in AECM vaccine.

Given that $CD8^+$ and $CD4^+$ T-cells are activated by MHC-I and MHC-II restricted antigens respectively, the above results also underscore the importance of $CD8^+$ T-cells. For a further determination, we depleted $CD8^+$ and $CD4^+$ T-cells using antibodies to assess their contribution, and found that the anti-tumour effect of AECM@PC7A was substantially abrogated by CD8 depletion in both B16-OVA and CT26 tumour models, while CD4 depletion displayed a negligible impact (Fig. 4k and Supplementary Fig. 8a–c). Hence, these findings demonstrated the necessity of MHC-I restricted antigens and the central role of $CD8^+$ T-cells in the anti-tumour response elicited by AECM@PC7A.

Since DCs are the major APC subtype for AECM vaccine to elicit T-cell response (Fig. 2l, m), we then investigate how DCs present AECM antigens to prime T cells. Apart from the canonical cross-presentation pathway that utilises APC's own MHC, APCs can also display exogenous MHC-peptide complex (pMHC) acquired from cells or extracellular vehicles (EVs), a process known as cross-dressing[53–55]. To determine which pathway DCs employ to present AECM antigens, we incubated AECM@PC7A of B16-OVA cells with $B2m^{-/-}$ DCs and found that MHC-I can be clearly detected on these MHC-I deficient DCs (Fig. 4l, m). When the AECM@PC7A treated DCs cells were washed extensively to eliminate the residual soluble vaccine and then co-cultured with OT-I T-cells, $B2m^{-/-}$ DCs induced substantial $CD8^+$ T-cell proliferation as well as WT DCs (Fig. 4n and Supplementary Fig. 8d), indicating that pMHC-I of AECM vaccine can be effectively transferred to the DC surface to prime T-cells. In contrast, PC7A-OVA and PC7A-Cell_lysate vaccines failed to stimulate T-cell priming when the DCs lacked MHC-I (Fig. 4o and Supplementary Fig. 8e). For further validation in vivo, we adoptively transferred OT-I T-cells into $B2m^{-/-}$ mice and then vaccinated them with AECM@PC7A or PC7A-OVAp. Consistently, PC7A-OVAp had negligible effect, whereas AECM@PC7A retained high activity to stimulate robust OT-I T-cell proliferation, reaching a level comparable to that observed in WT mice (Fig. 4p). AECM@PC7A did not trigger T-cell response in cDC1-deficient $Baft3^{-/-}$ mice (Figs. 2l and 3o), thereby excluding the possibility of direct T-cell activation by the vaccine. Taken together, these results highlighted the critical role that DC cross-dressing plays in enabling the AECM vaccine to initiate T-cell priming.

https://doi.org/10.1038/s41467-025-59977-8

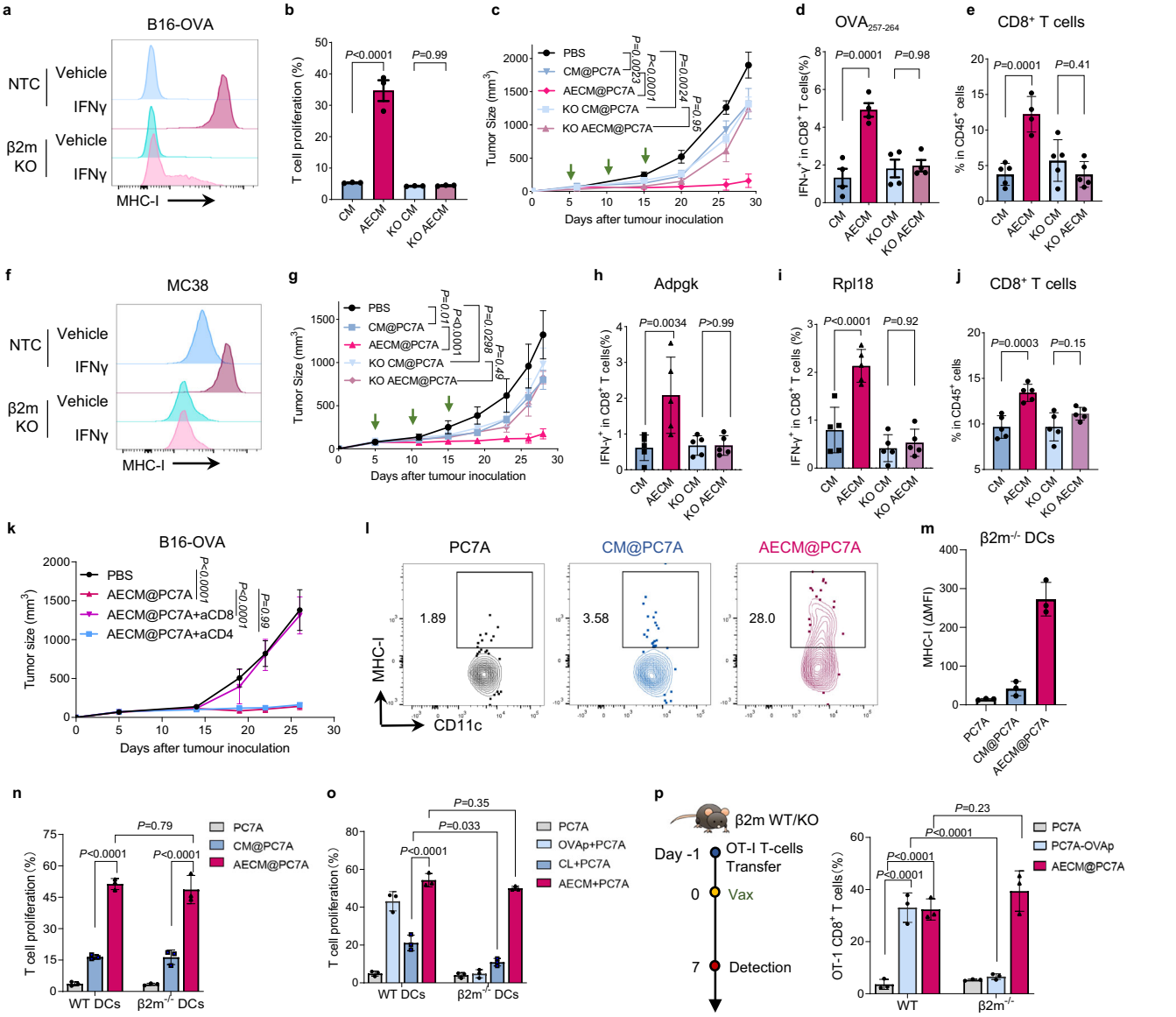

Fig. 4 | IFN-γ stimulates antigen enrichment in a MHC-I dependent manner. **a** Representative histograms showing OVA presentation on WT and *B2m*$^{-/-}$ B16-OVA cells upon IFN-γ treatment. **b** The abilities of CM and AECM from WT and *B2m*$^{-/-}$ B16-OVA cells (2 μg/mL) to stimulate OT-I T-cell proliferation (n = 3 independent experiments/group). **c**–**e** B16-OVA tumour growth curves were shown (**c**, n = 5 mice/group). At day-29 post tumour inoculation, PBMCs were re-stimulated and the IFN-γ secretion by CD8$^+$ T-cells were determined by ICS (**d**, n = 4 mice/group), and tumour infiltrating CD8$^+$ T-cells (**e**, n = 4 mice for AECM@PC7A group, n = 5 mice for other groups) were measured. **f** Representative histograms showing MHC-I expression on WT and *B2m*$^{-/-}$ MC38 cells upon IFN-γ treatment. MC38 tumour growth curves were shown (**g**, n = 5 mice/group). At day-28 post tumour inoculation, the IFN-γ secretion by CD8$^+$ T-cells in PBMCs upon re-stimulation with Adpgk (**h**) or Rpl18 (**i**) neoantigen peptide was determined by ICS, and tumour infiltrating CD8$^+$ T-cells (**j**) were measured (n = 5 mice/group). **k** B16-OVA tumour-bearing mice were i.t. vaccinated (black arrows), and received i.p. treatment of CD4, CD8 or isotype antibodies. Tumour growth curves were shown (n = 5 mice/group). **l**–**n** Splenic DCs were treated with B16-OVA derived nanovaccines (20 μg/mL) for 18 h, and MHC-I acquisitions was determined. Representative scatter plots (**l**) and the levels of acquired MHC-I as calculated by subtracting the MHC-I MFI from that of the untreated cells (**m**) for *B2m*$^{-/-}$ DCs were shown. The treated DCs were harvested and co-cultured with OT-I T-cells for 48 h, CD8$^+$ T-cell proliferation (**n**) were determined (n = 3 independent experiments/group). **o** Splenic DCs were treated with indicated PC7A vaccines for 18 h. The treated DCs were harvested and co-cultured with OT-I T-cells for 48 h, CD8$^+$ T-cell proliferation was measured (n = 3 independent experiments/group). **p** WT or *B2m*$^{-/-}$ mice were adoptively transferred with 2×10^5 OT-I T-cells, followed by s.c. vaccination 18 h later. The percentage of OT-1 CD8$^+$ T-cells (CD8$^+$OVA Tetramer$^+$) in spleens was determined (n = 3 mice/group). In (**b**–**e**, **g**–**k**, **m**–**p**), q representative data from three independent experiments are presented as means ± s.e.m. Source data are provided as a Source Data file.

Characteristics of AECM@PC7A induced anti-tumour response

To evaluate the efficacy of AECM@PC7A against distal tumour, lung metastasis was established as we described before[37]. B16-OVA cells were inoculated subcutaneously on the flanks of mice to induce primary tumours and then injected intravenously 4 days later to induce lung metastasis. AECM@PC7A vaccination by three dosages not only inhibited the growth of primary tumours substantially as expected (Fig. 5a, b), but also significantly reduced the number of lung metastasis lesions compared to CM@PC7A and control treatments (Fig. 5c, d).

The long-term immune memory effect was also investigated. B16-OVA tumour-free mice after AECM@PC7A vaccination in Fig. 3b were rechallenged with B16-OVA cells at day-80 post initial tumour inoculation. No tumour was found in these mice, in contrast to rapid tumour growth in naïve mice (Fig. 5e, f). Accordantly, the proportions of effector memory T-cells (T_{EM}, CD3$^+$CD8$^+$CD44$^+$CD62L$^-$) and central

https://doi.org/10.1038/s41467-025-59977-8

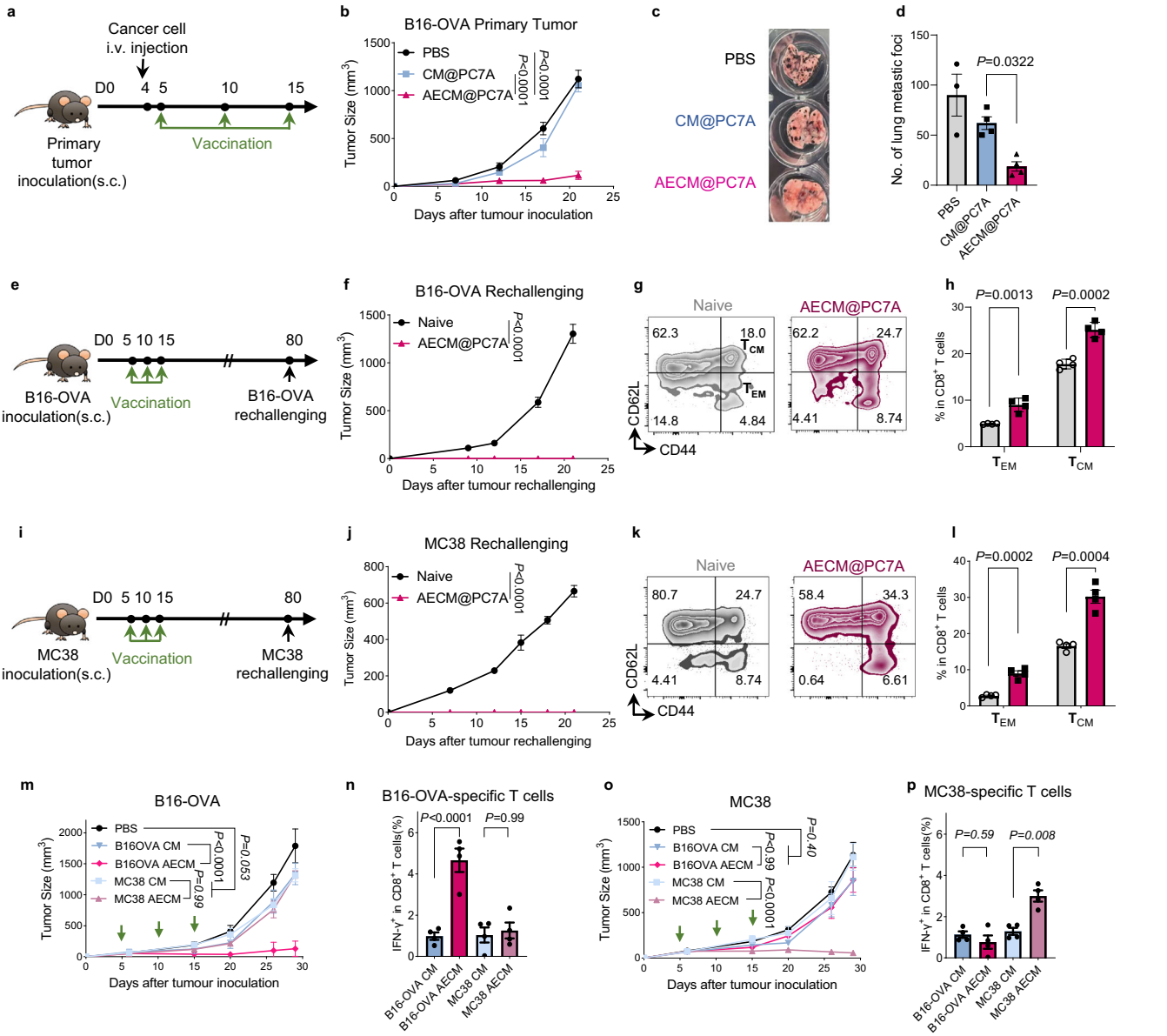

Fig. 5 | Characteristics of AECM@PC7A induced anti-tumour response. **a**–**d** C57BL/6 mice were s.c. inoculated with 1.5×10^5 B16-OVA cells on day-0 and intravenously injected with 1×10^5 B16-OVA cells on day-4, then received intratumoral vaccination at the primary tumour site on days 5, 10 and 15 (**a**). Growth curves of primary tumours (**b**, n = 4 mice/group), and the representative images (**c**) and quantification (**d**, n = 3 mice for PBS group, n = 4 mice for @PC7A groups) of lung metastasis at day-21 were shown. **e**–**h** B16-OVA tumour-free mice after AECM@PC7A vaccination were rechallenged with 1.5×10^5 B16-OVA cells (**e**). Tumour growth curves (**f**) and the representative scatter plots (**g**) and quantification (**h**) of T_{EM} and T_{CM} in the splenocytes at day-21 post rechallenge were shown (n = 4 mice/group). **i**–**l** MC38 tumour-free mice after AECM@PC7A vaccination were rechallenged with 2.5×10^5 MC38 cells (**i**). Tumour growth curves (**i**), and the representative scatter plots (**k**) and quantification (**l**) of T_{EM} and T_{CM} in the splenocytes at day-21 post rechallenge were shown (n = 4 mice/group). **m**, **n** B16-OVA tumour-bearing mice were treated with @PC7A nanovaccines derived from B16-OVA or MC38 cells. Tumour growth curves were shown (**m**, n = 5 mice/group), and the IFN-γ secretion by $CD8^+$ T-cells in splenocytes after re-stimulation with irradiated B16-OVA cells was determined by flow cytometry (**n**, n = 4 mice/group). **o**, **p** MC38 tumour-bearing mice were treated with @PC7A nanovaccines derived from MC38 or B16-OVA cells. Tumour growth curves were shown (**o**, n = 5 mice/group), and the IFN-γ secretion by $CD8^+$ T-cells in splenocytes after re-stimulation with irradiated MC38 cells was determined by flow cytometry (**p**, n = 4 mice/group). In (**b**, **d**, **f**, **h**, **j**, **l**, **m**–**p**) representative data from three independent experiments are presented as means ± s.e.m. Statistical significance was calculated by ordinary one-way ANOVA (**b**, **d**, **m**–**p**) or Student's two-sided unpaired t-test (**f**, **h**, **j**, **l**). Source data are provided as a Source Data file.

memory T-cells (T_{CM}, $CD3^+CD8^+$ $CD44^+CD62L^+$) in mouse splenocytes were notably higher in AECM@PC7A vaccinated mice than in naïve mice (Fig. 5g, h). Similar rechallenging outcomes were observed in the MC38 tumour model (Fig. 5i–l), indicating that AECM@PC7A nanovaccines could induce long-term memory response against tumour.

To determine whether the anti-tumour efficacy of AECM@PC7A was specific to its oriented cancer cell, we immunised B16-OVA tumour-bearing mice with AECM@PC7A vaccine derived from MC38 cells (Fig. 5m). In contrast to its significant inhibition on the growth of MC38 tumours (Fig. 3g, h), the MC38 AECM@PC7A vaccination did not inhibit the growth of B16-OVA tumours in mice (Fig. 5m), and no OVA-specific $CD8^+$ T-cell response was observed (Fig. 5n). Conversely, B16-OVA AECM@PC7A also did not inhibit the growth of MC38 tumours, and generated limited $CD8^+$ T-cell response (Fig. 5o, p). Therefore, AECM@PC7A elicited anti-tumour response specific to its oriented cancer cell type, offering a potential strategy for personalised cancer treatment.

https://doi.org/10.1038/s41467-025-59977-8

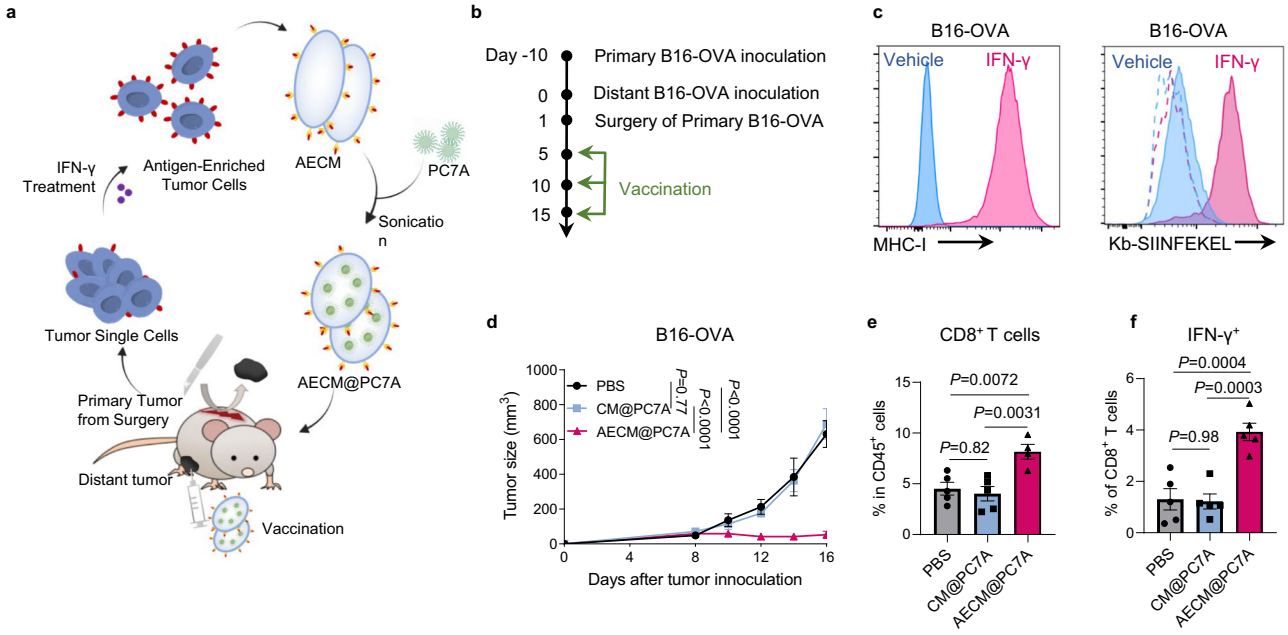

Fig. 6 | Anti-tumour effects of AECM@PC7A in post-surgical distant tumour model. Scheme (**a**) and timeline (**b**) to show the preparation of AECM@PC7A nanovaccine from surgically resected primary tumours for personalised treatment on distal tumours. **c** Representative histograms showing MHC-I expression on B16-OVA cells from resected primary tumours post IFN-γ treatment. Dashed lines, isotype; solid lines, anti-Kb-SIINFEKEL. **d** Distant tumour growth curves by different vaccinations (n = 5 mice/group). **e** Tumour-infiltrating $CD8^+$ T-cells at day-16 post distant tumour inoculation (n = 4 mice for AECM@PC7A group, and n = 5 mice for other groups). **f** The IFN-γ secretion by $CD8^+$ T-cells of PBMCs after re-stimulation with $OVA_{257-264}$ peptide was determined by flow cytometry (n = 5 mice/group). In (**d**–**f**) representative data from three independent experiments are presented as means ± s.e.m. Statistical significance was calculated by ordinary one-way ANOVA. Source data are provided as a Source Data file.

AECM@PC7A suppresses post-surgical distant tumours

To date, surgery represents the primary treatment option for most solid tumours, however, local recurrence and distant metastasis remain significant barriers for complete tumour control. To evaluate the potential of AECM@PC7A strategy in this clinical scenario, nanovaccines were formulated using surgically resected tumours (Fig. 6a). C57BL/6 mice were S.C. inoculated with B16-OVA cells on one flank first then on another flank 10 days later, and the first primary tumours were surgically resected 11 days after inoculation for IFN-γ treatment to generate the AECM@PC7A vaccine (Fig. 6b). As shown in Fig. 6c, IFN-γ treatment still increased MHC-I expression and OVA presentation significantly on the primary tumour cells. Following three AECM@PC7A vaccinations, distal tumour growth was substantially suppressed when compared to CM@PC7A and control treatments (Fig. 6d). Consistently, the number of tumour-infiltrating $CD8^+$ T-cells was significantly elevated in AECM@PC7A treated mice (Fig. 6e and Supplementary Fig. 9), and the IFN-γ^+ $CD8^+$ T-cells in the PBMCs from these mice were significantly increased upon OVA restimulation (Fig. 6f), demonstrating successful establishment of tumour-specific immune responses by post-operative AECM@PC7A vaccination.

AECM@PC7A suppresses humanised CDX model

We further evaluated the clinical potential of AECM@PC7A nanovaccine with a humanised cell line-derived xenograft (CDX) tumour model using MDA-MB-231, a human breast cancer cell line often used in CDX model, expressing HLA-A*02 (02:01, 02:17) subtype that at the highest frequency across all ethnic populations[56,57]. Similarly, IFN-γ treatment significantly increased HLA-I surface expression on these cells (Fig. 7a). To establish the CDX model, NSG mice were first I.V. injected with human PBMCs with HLA-A*02 (02:01, 26:01) subtype to generate a human immune system, followed by subcutaneous inoculation of MDA-MB-231 cells. The mice were injected with two dosages of nanovaccine from day 7 post-xenograft when tumours reached 40–60 mm^3 (Fig. 7b). AECM@PC7A vaccination substantially suppressed tumour growth, with 40% of mice achieving tumour regression, whereas no regression was observed in CM@PC7A vaccinated and control mice (Fig. 7c–e). In addition, when the $CD8^+$ T-cells from PBMCs of these mice were exposed to irradiated MDA-MB-231 cells, the proportion of IFN-γ^+ cells was highest in the AECM@PC7A group, indicating a potent tumour specific T-cell response induced by AECM@PC7A vaccination (Fig. 7f). Moreover, TME analysis revealed increased infiltration of human $CD45^+$ immune cells as well as $CD8^+$ T-cells in the tumour of AECM@PC7A vaccinated mice (Fig. 7g, h). These results demonstrated the effective anti-tumour efficacy elicited by AECM@PC7A in humanised CDX model, suggesting the potential of this strategy for clinical personalised cancer treatment.

Discussion

The uncertainty of neoantigen discovery and particularly the time-consuming procedure considerably restricted the therapeutic window and the widespread application of cancer vaccine in clinical practice[10]. In this study, aiming to address this pressing clinical need, we have developed the AECM strategy that using IFN-γ to stimulate antigen presentation, and the resulting tumour cell membranes can provide adequate tumour responsive antigens for PC7A vaccines to induce strong poly-epitopic anti-tumour CTL responses in multiple tumour models (Supplementary Fig. 10). AECM@PC7A exhibits superior anti-tumour efficacy when compared to the vaccines derived from normal cancer cell membrane, whole cell lysate, and characterised peptides. Moreover, preparation of AECM@PC7A vaccine takes only ~10 days, compared to ~3 months for neoantigen discovery-based vaccines, making it a versatile platform for personalised cancer vaccine design to overcome neoantigen identification challenges in a rapid and effective way.

The present work illustrates the potential of AECM based vaccine strategy for a broad range of cancer patients. Antigen presentation is regulated by multiple pathways, including those of IFN-γ, NF-κB, MEK and EGFR[39–42]. Our screen provides a map of MHC-I stimulators within

https://doi.org/10.1038/s41467-025-59977-8

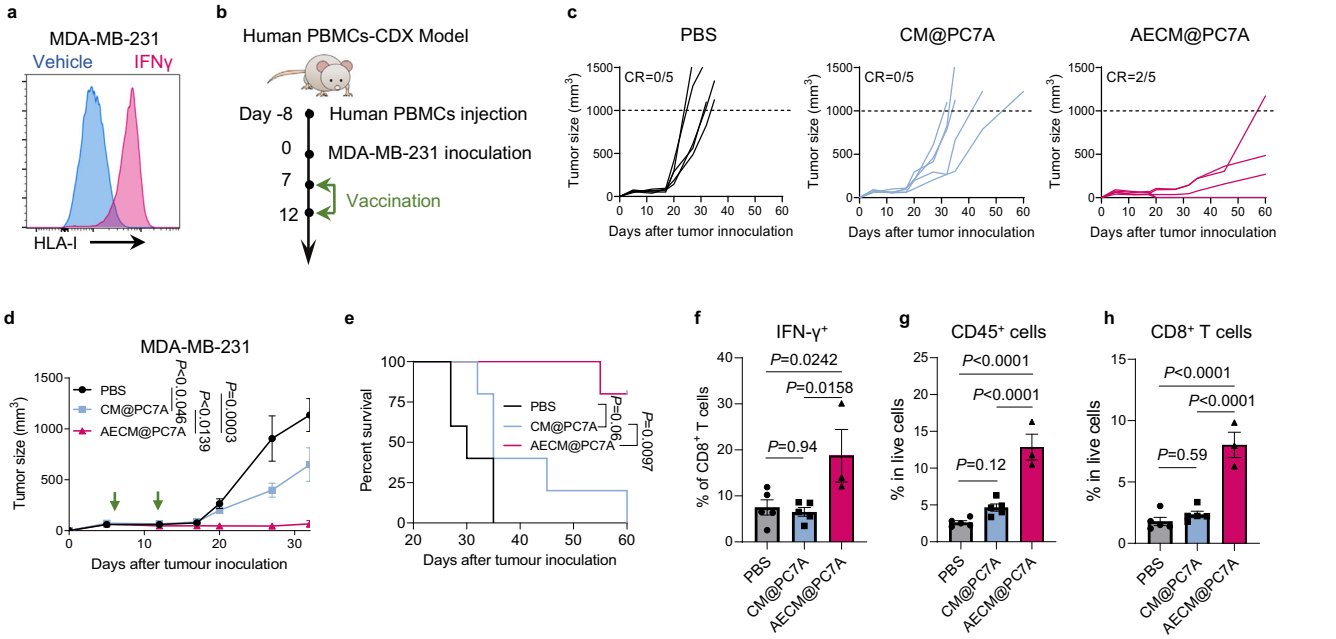

Fig. 7 | Anti-tumour effects of AECM@PC7A in a humanised CDX model. **a** Representative histogram showing HLA-I expression on IFN-γ treated and control MDA-MB-231 cells. **b** Scheme showing the model construction and the timeline of vaccination. NSG mice were injected intravenously with 5×10^6 human PBMCs for 8 days then inoculated with 2×10^6 MDA-MB-231 cells, followed by two doses of vaccinations. Individual (**c**) and average (**d**) tumour growth curves, and mice survival (**e**) of NSG mice with different treatments (**c**, **d**, n = 5 mice/group). **f** Irradiated cancer cell-reactive IFN-γ$^+$ cells in CD8$^+$ T-cells of PBMCs as determined by ICS (n = 3 mice for AECM@PC7A group, and n = 5 mice for other groups). The frequency of tumour infiltrating human immune cells (**g**) and CD8$^+$ T-cells (**h**) at day-28 post tumour inoculation. (**g**, **h**, n = 3 mice for AECM@PC7A group, and n = 5 mice for other groups). In (**d**, **f**–**h**, representative data from three independent experiments are presented as means ± s.e.m. Statistical significance was calculated by ordinary one-way ANOVA (**d**, **f**–**h**) and log-rank test (**e**). Source data are provided as a Source Data file.

FDA-approved drugs/cytokines, unveiling IFN-γ as a highly competitive stimulator for the antigen presentation across a wide spectrum of murine and human cancer cell types. IFN-γ receptor is expressed in nearly all nucleated cells[43,58]. Despite tumours employing multiple strategies to suppress the antigen presentation, our findings suggest that this suppression is often reversible, rendering IFN-γ-based AECM nanovaccines applicable to various cancer types. A minority of cancer cell types exhibit limited response to IFN-γ, and some cancer patients harbour genetic alterations encoding the IFN-gamma signalling pathway, accounting for ~5% of patients in the TCGA dataset[24]. To achieve the successful AECM strategy in such cases, other MHC-I stimulators identified in our screening may offer potential solutions.

Enrichment of MHC-I restricted antigens is essential for AECM vaccine to elicit anti-tumour response. AECM vaccines from MHC-I deficient cancer cells fail to suppress tumours, and the anti-tumour effects of AECM vaccines are almost completely abolished by CD8 depletion, demonstrating the necessity of MHC-I antigens and the central role CD8$^+$ T-cell plays. Although similar to conventional vaccines in these aspects, the process of antigen presentation to prime T-cells differs. DCs/APCs cross-present antigens from conventional vaccine via their own MHC-I, a mechanism that is fully abrogated when DCs lack MHC-I. Whereas, MHC-I deficient DCs can acquire the pMHC from AECM to prime T-cells robustly both in vitro and in vivo. Considering the complexity of antigen uptake, epitope processing and loading to MHC-I, the antigen presenting efficiency of cross-presentation is regarded as lower than that of cross-dressing which directly utilises the acquired pMHC-I[53–55]. This notion is further supported by our observation that AECM@PC7A elicits a stronger anti-tumour response than the PC7A-peptide vaccine, even when the latter contains much more purified antigen peptides. Our results also suggests that AECM antigens are predominantly presented by DCs via cross-dressing rather than the conventional cross-presentation. Multiple factors likely determine the extent to which MHC-I cross-dressing occurs and contributes to T cell priming. Intuitively, the abundance of MHC-I in donors must be important[53]. Given the abundance of pMHC-I on AECM and the high presenting potential of cross-dressing, it is plausible that AECM vaccine can trigger remarkable potency when compared to those derived of CM or whole cell lysates.

The APC subsets that is responsible to present antigens via cross-dressing remains controversial. Our data highlight the pivotal role of Batf3-dependent cDC1s in the process of pMHC-I cross-dressing. This aligns with cDC1s' endosomal biology. Unlike other APCs, which generate acidic endosomal for pathogen degradation, cDC1s maintain a neutral pH that stabilises pMHC-I complexes, enabling their recycling to the cell surface[59–63]. Given that cDC1s, cDC2s, and more recently monocytes have all been shown to be capable of acquiring pMHC-I complex to initiate anti-viral or anti-tumour CD8$^+$ T-cell responses[64–66], it appears that different APC subsets may exhibit a bias towards MHC-dressing under different situations. Further investigation is required to elucidate the underlying mechanism.

Recently, APC-based membrane nanoparticles have been developed, such as ASPIRE strategy. ASPIRE uses the cell membranes of DCs with overexpressed antigens, co-stimulatory signals, and immune suppression reversal molecules to elicit strong anti-tumour immune responses and overcome stubborn immune tolerance[67]. Similar to many other cancer vaccines, precise neoantigens or TAAs are required for design of ASPIRE. A unique feature of ASPIRE is the direct activation of T-cells in a DC-like manner, enabling anti-tumour response without the need of DC maturation. Although AECM can also directly activate T-cells in vitro, the T-cell response relies on DC cross-dressing and does not occur in *Batf-3* KO mice deficient in DCs. Certain peptide-derived epitopes processed by professional APCs may not be displayed efficiently within a tumour cell, as immune and non-immune cells express diverse proteasomal subunits, yielding distinct peptidomes for MHC presentation[24,68]. Thus, cross-dressing might not only quantitatively enhance tumour antigen presentation, but also enable

DCs to more faithfully and effectively mirror the cancer cell peptidome[53–55], making the AECM strategy hold great potential to stimulate T-cell responses against a more diverse array of tumour-responsive antigens and representing a valuable addition to existing therapeutic modalities.

Among the enriched MHC-I antigens, despite tolerogenic self-antigens, the neoantigens and the weak immunogenic tumour associated antigens (TAAs) would synergistically contribute to the anti-tumour effects of AECM vaccines. MS-based immune-peptidomes serves as potent approaches for identifying HLA-bound neoantigen and TAAs[69–72]. However, due to the low HLA-I levels in tumour cells and the limitation of MS sensitivity, cancer epitopes with low copies are hard to be identified[9]. AECM, with substantially increased HLA-I antigen presentation, thereof, will also provide a feasible platform to more effectively identify the precise neoantigens or TAAs for cancer treatment.

In conclusion, this proof-of-concept study has demonstrated that the Antigen-Enriched Cell Membrane coated PC7A nanovaccine is capable of triggering robust poly-epitopic T-cell responses, resulting in significant tumour regression, metastasis prevention, and long-term immune memory in various murine and humanised cancer models, offering a promising and universal avenue for the rapid development of personalised cancer vaccines.

Methods

Ethics declarations

This research complies with all relevant ethical regulations. All animal procedures were performed with ethical compliance and approval by the Institutional Animal Care and Use Committee (IACUC) at Fudan University. Tumour-bearing mice were humanely euthanized immediately upon observation of tumours exceeding 2000 mm^3, in full compliance with the approved protocol. The use of human PBMC samples in this study was approved by the Ethics Committees at the Shanghai Liquan Hospital.

Mice

Wild-type C57BL/6 and BALB/c mice were purchased from GemPharmatech (Shanghai, China). C57BL/6Smoc-*Batf3*^{em1Smoc} mice and NOD-*Prkdc*^{scid}*Il2rg*^{em1}/Smoc mice were purchased from Shanghai Model Organisms Center (Shanghai, China). All mice were maintained under specific pathogen-free conditions at 22–26 °C with a 12:12 h dark/light cycle and 40–70% humidity. For experiments with wild-type C57/BL6 mice, *B2m*$^{-/-}$ mice, *Batf3*$^{-/-}$ mice, NSG mice and wild-type BALB/c mice, female mice with age between 6 and 8 weeks were used. For experiments with OT-1 TCR transgenic mice, female and male mice between age 6–12 were used. Tumour growth was monitored two to three times a week. Mice were euthanized immediately upon detection of tumours exceeding 2000 mm^3, and the terminal measurements were systematically recorded and incorporated into the experimental dataset. All experiments were performed in accordance with the protocol approved by the IACAU of Fudan University.

Peptides

$OVA_{257–264}$ peptide was purchased from Genscript (Nanjing, China). $Gp70_{423-431}$(AH1, SPSYVYHQF), $Gp100_{21–41}$ (VGALEGSRNQDWLGVP RQLVT), $Trp1_{214–237}$ (SHEGPAF LTWHRYHLLQLERDMQE), $Trp2_{173–196}$ (QPQIANCSVYDFFVWLHYYSVRDT), B16-M27(REGVELCPGNKYEMRR HGTTHSLVIHD), B16-M33 (DSGSPFPAAVILRDALH MARGLKYLHQ), $Rpl18_{115-132}$ (KAGGKILTFDRLALESPK), $Adpgk_{R304M}$ (GIPVHLELA SMTN MELMSSIVHQQVFPT), and CT26-M19 (QAIVRGCSMPGPWRSGRLLVS RR WSVE) were synthesised by Genscript (Nanjing, China).

Cell culture

All cells were cultured in a constant temperature incubator at 37 °C in the presence of 5% CO_2 and normal levels of O_2. B16-F10 (mouse, melanoma, TCM36), MC38 (mouse, colon carcinoma, SCSP-5431), LLC (mouse, Lewis lung carcinoma, SCSP-5252), EL4 (mouse, lymphoma, SCSP-5221), MDA-MB-231 (human, breast cancer, TCHu227), T47D (human, breast cancer, SCSP-564), U251 (human, glioma, TCHu58,), WERI-Rb-1 (human, retinoblastoma, TCHu213), Huh-6 (human, hepatocellular carcinoma, TCHu181), Huh-7 (human, hepatocellular carcinoma, TCHu182), PLC/PRF/5 (human, hepatocellular carcinoma, TCHu119), MG63 (human, osteosarcoma, TCHu124), Hep3B2.1-7 (human, hepatocellular carcinoma, TCHu106), NCl-H1703 (human, lung squamous cell carcinoma, SCSP-593), SH-SY5Y (human, neuroblastoma, TCHu97), FaDu (human, head and neck squamous cell carcinoma, TCHu132), HT1080 (human, fibrosarcoma, TCHu170), SNU-1 (human, gastric cancer, TCHu242), SK-MEL-28 (human, melanoma, SCSP-5223), HEK293T (human, embryonic kidney cells, GNHu48), Colo205 (human, colon carcinoma, TCHu102), RBE (human, cholangiocarcinoma, TCHu179), 786-O (human, renal cell carcinoma, TCHu186), CT26 (mouse, colon carcinoma, TCM37), SK-BR-3 (human, breast cancer, TCHu225), SW620 (human, colon carcinoma, TCHu101) were purchased from National Collection of Authenticated Cell Cultures. QBC939 (human, cholangiocarcinoma, SNL-186) were purchased from Sunncell (Wuhan, China). SEM (human, acute lymphoblastic leukemia, ACC 546) were purchased from DSMZ (Germany). B16-OVA (mouse, melanoma, MZ-8054), TC1 (mouse, HPV16 E6/E7-expressing tumour cell line, MZ-2879), Pan-02 (mouse, pancreatic carcinoma, MZ-0732), NOMO-1 (human, acute myeloid leukemia, MZ-8200), MOLM13 (human, acute myeloid leukemia, MZ-336130), SUM-159 (human, breast cancer, MZ-2427), Hey (human, ovarian cancer, MZ-8049), HT-144 (human, melanoma, B164800) and Py8119 (mouse, breast cancer, MZ-8063) were purchased from Mingzhou-bio (Hangzhou, China). For cell culture, MDA-MB-231, QBC939, T47D, U251, WERI-Rb-1, Huh-6, Huh-7, PLC/PRF/5, MG63, Hep3B2.1-7, NCl-H1703, SH-SY5Y, FaDu, Hey, HT1080, HT-144, SNU-1, SK-MEL-28, HEK293T, B16-F10, B16-OVA, LLC, Pan-02 and MC38 cells were cultured in DMEM medium. NOMO-1, MOLM13, SUM-159, Colo205, SEM, RBE, 786-O and CT26 cells were cultured in RPMI 1640 medium. SK-BR-3 cells were cultured in McCoy's 5 A medium. SW620 cells were cultured in Leibovitz's L-15 medium. Py8119 cells was cultured in F12 medium (Gibco) with 1 μg/ml hydrocortisone (Sigma), 50 μg/ml gentamicin (Sigma), 10 ng/mL epidermal growth factor (PeproTech) and 5 μg/ml insulin (Biosharp Life Science). All media were supplemented with 10% FBS and 1% penicillin and streptomycin (Thermo Fisher, 100×). All cell lines were authenticated using STR profiling at least once every two years from receipt, and were tested routinely using a mycoplasma contamination kit (R&D Systems) and confirmed negative prior to experiments.

Screening for MHC-I stimulators

A library containing 1738 FDA-approved small molecule drugs and 50 cytokines was used for screening. B16-OVA cells or other indicated cells were treated with each drug or cytokine at dose of 1 μM or 10 ng/mL for 48 h, respectively. For MHC-I stimulator screening, PE anti-mouse H2-kb/H2-Db (Biolegend, clone: 28-8-6) and anti-mouse H-2Kb bound to SIINFEKL Antibody (Biolegend, clone: 25-D1.16) were used to detect MHC-I expression and OVA presentation. DAPI (Beyotime) was used to distinguish live cells from the dying or dead cells. MHC-I expression and cell viability were measured by HTS flow cytometry (BD Canto II) and were analyzed with FlowJo software.

Preparation of AECM@PC7A vaccine

To obtain cancer cell membranes, the indicated cells were cultured with/without IFN-γ (10 ng/ml) treatment for 48 h, and then were collected by a cell scraper and centrifuged at 700 g for 5 min. After washed with PBS, the obtained cell pellets were suspended in a hypotonic lysis buffer containing membrane protein extraction reagent and phenylmethanesulfonyl fluoride according to the manufacturer's instructions (Beyotime, P0033). Thereafter, repeated freeze-

thawing was carried out and then centrifuged at 700 g for 10 min at 4 °C to remove nucleoprotein. The collected supernatant was further centrifuged at 14,000 g for 30 min to collect the cell membranes. The membranes were separated in normal saline prior to use.

To generate CM@PC7A or AECM@PC7A nanoparticles, the cell membrane was resuspended in saline, mixed with PC7A polymer and diluted with saline to a final concentration of 1 mg of membranes and 300 μg of PC7A NP per mL. Then the mixture was sonicated for 2 min in ultrasonic bath sonicator (Anonkia). The nanoparticles were characterised by dynamic light scattering (Malvern MicroV model, He-Ne laser, λ = 632 nm) to determine the hydrodynamic diameter and polydispersity index.

Western blotting

Samples were separated by SDS-PAGE and transferred to nitrocellulose membranes. The membrane was labelled with the primary antibody and then to the HRP-conjugated secondary antibody at the suggested concentration and detected with an ECL kit (Beyotime). Anti-HLA-C (15777-1-AP) polyclonal antibodies were obtained from ProteinTech Group (Chicago, Ill). Anti-Sodium Potassium ATPase Rabbit Monoclonal Antibody (AF1864), anti- Histone H3 Mouse Monoclonal Antibody (AF0009), anti−β-Tubulin rabbit monoclonal antibody (AF1216), HRP−labelled goat anti-mouse IgG (H + L) (A0216), and HRP−labelled goat anti-rabbit IgG (H + L) (A0208) were obtained from Beyotime. Uncropped and unprocessed scans of the important blots were provided in the Source Data file.

Flow cytometry

Subcutaneous tumour tissues were digested with PBS containing 2% FBS and collagenase type IV (0.25 mg/mL, Sigma) and DNase I (20 U/mL, Sigma). Cells were placed on a shaker and incubated for 20 min at 37 °C. After 10 min of incubation, tumour particles were pipetted vigorously by use of a 10-mL pipette to enhance disaggregation. Then the digested mixtures cells were filtered through a 70-μm nylon cell strainer. Spleens and lymph nodes were harvested under sterile conditions. Blood was harvested with heparin, and red blood cells were removed using RBC lysis buffer. Cells were washed, blocked with FACS buffer containing anti-mouse CD16/32 (Biolegend, clone: 93). For surface staining, PE antimouse H2-kb/H2-Db (Biolegend, clone: 28-8-6), FITC antihuman HLA-A/B/C (Biolegend, clone: W6/32), PE-Cy7 antimouse B220 (Biolegend, clone: RA3-6B2), Pacific Blue antimouse/human CD11b (Biolegend, clone: M1/70), Brilliant Violet 510 antimouse CD11c (Biolegend, clone: N418), FITC antimouse CD3 (Biolegend, clone: 145−2 C11), APC-Cy7 antimouse CD4 (Biolegend, clone: GK1.5), BV510 antimouse CD45 (Biolegend, clone: 30-F11), APC antimouse CD45 (Biolegend, clone: 30-F11), APC antimouse CD49b (Biolegend, clone: DX5), PE antimouse CD69 (Biolegend, clone: H12F3), eFluor 450 antimouse CD8a (Biolegend, clone: 53−6.7), APC antimouse CD8a (Biolegend, clone: 53−6.7), PE-Cy7 antimouse CD86 (Biolegend, clone: GL-1), FITC antimouse CD80 (Biolegend, clone: 16-10A1), FITC antimouse Ly-6C (Biolegend, clone: HK1.4), APC/Cy7 anti-mouse Ly-6G (Biolegend, clone: 1A8) and PE antimouse MHCII (Biolegend, clone: M5/114.152.2) were used. Immune subpopulations were determined as previously described[73]. For tetramer staining, cells were stained with H-2Kb OVA Tetramer-SIINFEKL-PE (MBL International) and FITC antimouse CD8 antibody (MBL International). For T cell memory phenotyping, cells were stained with PE antimouse CD62L (Biolegend, clone: W18021D) and APC antimouse CD44 (Biolegend, clone: IM7). We used 7-AAD (BioLegend) to distinguish live from dying or dead cells. Cells were washed, and the final suspension analyzed by flow cytometry. Flow cytometry data were acquired on a BD LSR II flow cytometer and analyzed using FlowJo software.

Haemolysis assay

The capacity of polymers to promote pH-dependent disruption of lipid bilayer membranes was assessed by a RBC haemolysis assay as previously described[35]. Briefly, nanoparticles (30 μg/mL PC7A or 100 μg/mL CM@PC7A) were incubated mouse erythrocytes for 1 h at 37 °C in 100 mM sodium phosphate buffer (supplemented with 150 mM NaCl) under the pH range of the endosomal processing pathway (7.4, 7.2, 7.0, 6.8 and 6.6). The extent of cell lysis (that is, haemolytic activity) was determined spectrophotometrically by measuring the amount of haemoglobin released (Abs at 541 nm). Haemolytic activity was normalised to 100% lysis control (1% Triton X-100 treated RBCs). Samples were run in duplicate.

T-cell activation in vitro

C57BL/6-Tg (TcraTcrb)1100Mjb/J transgenic mice (OT-I) were euthanized and their spleens were collected. To obtain single cell suspensions, each spleen was physically extruded through a 70 μm nylon cell strainer (Fisher Scientific), followed by red blood cell removal using RBC lysis buffer (Biolegend). The cells were then washed with 1 × PBS, and were labelled with CellTrace™ Violet (0.5 μM concentration, 15 min in RPMI-1640) according to the manufacturer's instructions. Purified $CD3^+$ T-cells were obtained using flow cytometry sorter. 2×10^5 splenocytes or purified T-cells from OT-I mice were incubated with the indicated membrane at a concentration of 0, 0.2, 2 and 20 μg/mL for 3 days. Cells were cultured in complete RPMI-1640 medium supplemented with 10% FBS, 1 mM sodium pyruvate, 0.1 mM nonessential amino acids and 100 IU/mL penicillin, and 100 IU/mL streptomycin. The cells were collected 72 h later and stained with related antibodies for flow cytometry analysis. Proliferation of $CD8^+$ T-cells and CD69 surface marker expression were measured by using FACS Canto II Cell Analyzer (BD Biosciences). CTV-labelled splenocytes without OVA peptide stimulation were used as a control.

APC maturation and T-cell priming in vitro

For APC preparation, Bone marrow-derived dendritic cells (BMDCs) were obtained as previously described[35]. Briefly, tibiae and femurs of C57BL/6 mice were harvested and the bone marrow extracted by flushing media through the bones using a syringe equipped with a 26-gauge needle. Cells were passed through a 70 μm strainer to remove debris, washed, and plated. Complete media (RPMI supplemented on 10% FBS, 100 U/mL penicillin, 100 μg/mL streptomycin and 20 ng/mL GM-CSF) was supplemented on day 3. BMDCs were used on day 5 from the suspended and loosely-adhered cell population. In cross-dressing related assay, splenic DCs from C57BL/6 WT or $B2m^{-/-}$ mice were purified using anti-CD11c microbeads (130-125-835, Miltenyi Biotech) on MACS LS separation columns (Miltenyi Biotec) according to the manufacturer's instructions.

For T-cell priming, BMDCs or the splenic DCs (2×10^5 cells per well) were incubated with CM or its derived @PC7A nanovaccine at a indicated final concentration for 18 h in 96-well plates. BMDCs or purified splenic DCs were washed three times with PBS, followed by the addition of 2×10^5 CTV-labelled OT-1 splenocytes or the sorted T-cells per well. After 48 h of co-incubation, cells were collected and stained with the antibodies described above for flow cytometry. Data was collected using a Becton Dickinson FACS Canto II flow cytometer and analyzed using FlowJo.

Intracellular cytokine staining

Cells were subjected to intracellular cytokine staining with a staining buffer set (Invitrogen, Cat#:00−5523) according to the manufacturer's instructions. For IFN-γ staining, 5×10^5 cells were incubated with 1 μg/mL indicated antigenic peptide and 1 μg/mL brefeldin A for 6 h before intracellular cytokine staining. For intracellular cytokine staining, cells were labelled with anti-CD45-BV510, anti-CD3-ef450, anti-CD4-APC-Cy7 and anti-CD8-APC before membrane permeabilization and later intracellularly labelled with PE antimouse IFN-γ (clone: XMG1.2).

Immunisation and anti-tumour efficacy studies

For the prophylactic vaccination study and adjuvant test, C57BL/6 mice (n = 5 for each group) were injected subcutaneously with AECMs (100 μg) physically mixed with indicated adjuvant (30 μg) for 3 shots, followed by a challenge with 1.5×10^5 B16-OVA cells injected s.c. at the flank on day 15. For the therapeutic vaccination studies, C57BL/6 mice (n = 10 for each group) were injected subcutaneously with B16-OVA (1.5×10^5) cells, B16-F10 (1.5×10^5) cells or MC38 cells (2.5×10^5) into the right flank. BALB/c mice (n = 5 for each group) were injected subcutaneously with CT26 cells (1.5×10^5) into the right flank. Animals were immunised by either subcutaneous injection of the nanovaccine at the tail base or intratumoural injection of nanovaccine when the tumour size reaches 50–100 mm^3. Tumour growth was subsequently measured two times a week using a digital caliper and calculated as $0.5 \times length \times width^2$. Mice were considered humanely euthanized due to tumour burden when observation of tumours exceeding 2000 mm^3 or when adverse signs (such as pain, apathy, dehydration and necrotic tumour) were observed, and this event was recorded as death in the survival analysis (the end point of tumour detection is two times the longest survival time (LST) of the control group). For lung metastasis model, mice were injected subcutaneously with 1.5×10^5 B16-OVA cells and intravenously with 1.5×10^5 B16-OVA cells 4 days later, followed by three vaccinations at a dose of 300 μg per shot. Lung metastasis was analyzed at day 23 post intravenous injection. For the cell depletion assay, mice were given 200 μL of Clodronate-liposomes, 250 μg of anti-CD8a antibody or anti-CD4 antibody by I.P. injection every 4 days per mouse during vaccination. For in vivo adoptive transfer assay, 2×10^5 of sorted OT-1 T-cells were adoptively transferred into WT or $B2m^{-/-}$ mice. 18 h later, mice were vaccinated with PC7A-OVAp (1 μg peptide, 30 μg PC7A), AECM@PC7A(300 μg) or PC7A control(30 μg) by s.c. injection. Seven days post vaccination, spleens were harvested, and OT-1 cell proliferation was determined by flow cytometry. For post-surgery therapeutic study, B16-OVA cells were transplanted into the left flanks of C57BL/6 mice. After 10 days, the distant tumour (1.5×10^5 B16-OVA) was inoculated into the right flank of each mouse. At day 11, mice were randomly divided into three groups for different treatments. Tumours in the left flank of each mouse were surgically resected for collagenase type IV digestion, and the tumour cells were then cultured with or without IFN-γ (10 ng/ml) for 48 h to generate CM or AECM @PC7A nanoparticles. On 4, 9 and 14 days after surgery, the mice were intratumoural vaccinated with the corresponding nanoparticles with a dose of 300μg per shot. For human CDX model, 5×10^6 human PBMCs (Saily-bio, Shanghai, China) were injected intravenously into each NSG mouse. Peripheral blood from all mice was monitored for human immune cell ($hCD45^+$) reconstitution. 8 days later, the mice were injected subcutaneously with MDA-MB-231 cells (2×10^6) into the right flank. The mice were I.T. injected with two dosages of nanovaccine (300μg per shot) from day 7 post-xenograft when tumours reached 40–60mm^3.

ELISpot

ELISpot analysis was performed using the commercially available mouse IFN-γ ELISPOT set (Dakewe, 210005) following the manufacturer's instructions. Briefly, splenocytes were seeded in a 96 well plate (10^5 cells per well), pre-coated with a mouse anti-IFN-γ antibody and incubated with $OVA_{257\text{-}264}$ peptide for 20 h. A biotinylated antibody specific for IFN-γ and alkaline-phosphatase conjugated to streptavidin were subsequently used to detect the IFN-γ that secreted by the re-stimulated T cells. By adding a substrate solution, visual spots were formed at the sites of captured IFN-γ, and automated spot quantification was caried out by Dakewe Biotech.

CRISPR/Cas9 knockout of B2m

B2m guide RNA was constructed into lentiCRISPR v2 (Addgene #52961) with a targeting sequence of AGTATACTCACGCCACCCACCGG, and a non-targeting sequence of GTATTACTGATATTGGTGGG was set as control. The sgRNA plasmid was cotransfected with psPAX2 and pMD2G plasmids into HEK293T cells using Lipofectamine 2000 (Invitrogen) according to the manufacturer's protocol. Lentiviruses were collected 72 h post transfection, mixed with polybrene (Sigma-Aldrich) at a final concentration of 6 μg/mL, and added to the target cells. After 48 h of transduction, selection was performed by culturing the cells in media containing 4 μg /mL puromycin (Thermo Fisher).

Statistics and reproducibility

Summary graphs of data are presented with all data points to demonstrate data distribution. Statistical analysis was performed using Microsoft Excel and Prism 7.0 (GraphPad). representative data from three independent experiments are presented as means ± s.e.m. Data were analyzed by Student's t-test or one-way ANOVA. Based on pilot immunisation and tumour treatment studies, we used group sizes of 3–6 animals/group for immunogenicity measurements and 5–10 animals/group for tumour therapy experiments. No data were excluded from the analyses. For each experiment, tumour-bearing mice were randomised at the time when treatment started based on tumour size. For in vitro experiments, no randomisation is needed since the cells treated are from the same batch. The tumour measurement was performed with cage labels blinding for treatments. The in vitro experiments were executed and analyzed by different investigators in the lab.

Reporting summary

Further information on research design is available in the Nature Portfolio Reporting Summary linked to this article.

Data availability

Data generated in this study are provided in the Supplementary Information/Source Data file. Source data are provided with this paper.

References

1. Chen, D. S. & Mellman, I. Oncology meets immunology: the cancer-immunity cycle. *Immunity* **39**, 1–10 (2013).
2. Badrinath, S. et al. A vaccine targeting resistant tumours by dual T cell plus NK cell attack. *Nature* **606**, 992–998 (2022).
3. Liu, C. et al. mRNA-based cancer therapeutics. *Nat. Rev. Cancer* **23**, 526–543 (2023).
4. Chen, S. et al. Nanotechnology-based mRNA vaccines. *Nat. Rev. Methods Prim.* **3**, 63 (2023).
5. Zhang, R. et al. Manganese salts function as potent adjuvants. *Cell Mol. Immunol.* **18**, 1222–1234 (2021).
6. Lang, F., Schrörs, B., Löwer, M., Türeci, Ö & Sahin, U. Identification of neoantigens for individualized therapeutic cancer vaccines. *Nat. Rev. Drug Discov.* **21**, 261–282 (2022).
7. Pearlman, A. H. et al. Targeting public neoantigens for cancer immunotherapy. *Nat. Cancer* **2**, 487–497 (2021).
8. Yarchoan, M. et al. Targeting neoantigens to augment antitumour immunity. *Nat. Rev. Cancer* **17**, 209–222 (2017).
9. Bassani-Sternberg, M. et al. Direct identification of clinically relevant neoepitopes presented on native human melanoma tissue by mass spectrometry. *Nat. Commun.* **7**, 13404 (2016).
10. Xie, N. et al. Neoantigens: promising targets for cancer therapy. *Signal Transduct. Target. Ther.* **8**, 9 (2023).
11. Ott, P. A. et al. An immunogenic personal neoantigen vaccine for patients with melanoma. *Nature* **547**, 217–221 (2017).
12. Sahin, U. et al. Personalized RNA mutanome vaccines mobilize poly-specific therapeutic immunity against cancer. *Nature* **547**, 222–226 (2017).
13. Hilf, N. et al. Actively personalized vaccination trial for newly diagnosed glioblastoma. *Nature* **565**, 240–245 (2019).

14. Rojas, L. A. et al. Personalized RNA neoantigen vaccines stimulate T cells in pancreatic cancer. *Nature* **618**, 144–150 (2023).
15. Wells, D. K. et al. Key parameters of tumor epitope immunogenicity revealed through a consortium approach improve neoantigen prediction. *Cell* **183**, 818–834.e813 (2020).
16. Meng, Z., Zhang, Y., Zhou, X., Ji, J. & Liu, Z. Nanovaccines with cell-derived components for cancer immunotherapy. *Adv. Drug Deliv. Rev.* **182**, 114107 (2022).
17. Kroll, A. V., Fang, R. H. & Zhang, L. Biointerfacing and applications of cell membrane-coated nanoparticles. *Bioconjug. Chem.* **28**, 23–32 (2017).
18. Fusciello, M. et al. Artificially cloaked viral nanovaccine for cancer immunotherapy. *Nat. Commun.* **10**, 5747 (2019).
19. Liu, G. et al. Bacteria-derived nanovesicles enhance tumour vaccination by trained immunity. *Nat. Nanotechnol.* **19**, 387–398 (2024).
20. Le, D. T., Pardoll, D. M. & Jaffee, E. M. Cellular vaccine approaches. *Cancer J.* **16**, 304–310 (2010).
21. Le, D. T. et al. Safety and survival with GVAX pancreas prime and Listeria Monocytogenes-expressing mesothelin (CRS-207) boost vaccines for metastatic pancreatic cancer. *J. Clin. Oncol.* **33**, 1325–1333 (2015).
22. Tsujikawa, T. et al. Evaluation of Cyclophosphamide/GVAX Pancreas Followed by Listeria-Mesothelin (CRS-207) with or without Nivolumab in Patients with Pancreatic Cancer. *Clin. Cancer Res.* **26**, 3578–3588 (2020).
23. Pérez-Baños, A. et al. Whole tumour cell-based vaccines: tuning the instruments to orchestrate an optimal antitumour immune response. *Br. J. Cancer* **129**, 572–585 (2023).
24. Jhunjhunwala, S., Hammer, C. & Delamarre, L. Antigen presentation in cancer: insights into tumour immunogenicity and immune evasion. *Nat. Rev. Cancer* **21**, 298–312 (2021).
25. Li, S. Y. et al. Cancer cell membrane camouflaged cascade bioreactor for cancer targeted starvation and photodynamic therapy. *ACS Nano* **11**, 7006–7018 (2017).
26. Jin, J. et al. Human cancer cell membrane-coated biomimetic nanoparticles reduce fibroblast-mediated invasion and metastasis and induce T-Cells. *ACS Appl. Mater. Interfaces* **11**, 7850–7861 (2019).
27. Xu, J. et al. A general strategy towards personalized nanovaccines based on fluoropolymers for post-surgical cancer immunotherapy. *Nat. Nanotechnol.* **15**, 1043–1052 (2020).
28. Fang, R. H. et al. Cancer cell membrane-coated nanoparticles for anticancer vaccination and drug delivery. *Nano Lett.* **14**, 2181–2188 (2014).
29. Ochyl, L. J. et al. PEGylated tumor cell membrane vesicles as a new vaccine platform for cancer immunotherapy. *Biomaterials* **182**, 157–166 (2018).
30. Jiang, Y. et al. Engineered cell-membrane-coated nanoparticles directly present tumor antigens to promote anticancer immunity. *Adv. Mater.* **32**, e2001808 (2020).
31. Zaretsky, J. M. et al. Mutations associated with acquired resistance to PD-1 blockade in melanoma. *N. Engl. J. Med.* **375**, 819–829 (2016).
32. Yamamoto, K. et al. Autophagy promotes immune evasion of pancreatic cancer by degrading MHC-I. *Nature* **581**, 100–105 (2020).
33. Rizvi, N. A. et al. Cancer immunology. Mutational landscape determines sensitivity to PD-1 blockade in non-small cell lung cancer. *Science* **348**, 124–128 (2015).
34. Katsikis, P. D., Ishii, K. J. & Schliehe, C. Challenges in developing personalized neoantigen cancer vaccines. *Nat. Rev. Immunol.* **24**, 213–227 (2024).
35. Luo, M. et al. A STING-activating nanovaccine for cancer immunotherapy. *Nat. Nanotechnol.* **12**, 648–654 (2017).
36. Li, S. et al. Prolonged activation of innate immune pathways by a polyvalent STING agonist. *Nat. Biomed. Eng.* **5**, 455–466 (2021).
37. Jiang, X. et al. Intratumoral administration of STING-activating nanovaccine enhances T cell immunotherapy. *J. Immunother. Cancer* **10**, e003960 (2022).
38. Chen, Z. et al. 1155 ONM-501, a polyvalent STING agonist, exhibits anti-tumor efficacy with increased tumor T-cell infiltration in mice and is well tolerated in rats and non-human primates. *J. Immunother. Cancer* **10**, A1198 (2022).
39. Segars, J. H. et al. Retinoic acid induction of major histocompatibility complex class I genes in NTera-2 embryonal carcinoma cells involves induction of NF-kappa B (p50-p65) and retinoic acid receptor beta-retinoid X receptor beta heterodimers. *Mol. Cell Biol.* **13**, 6157–6169 (1993).
40. Lulli, D., Carbone, M. L. & Pastore, S. The MEK inhibitors trametinib and cobimetinib induce a type I interferon response in human keratinocytes. *Int. J. Mol. Sci.* **18**, 2227 (2017).
41. Mimura, K. et al. T cell recognition of HLA-A2 restricted tumor antigens is impaired by the oncogene HER2. *Int. J. Cancer* **128**, 390–401 (2011).
42. Pollack, B. P., Sapkota, B. & Cartee, T. V. Epidermal growth factor receptor inhibition augments the expression of MHC class I and II genes. *Clin. Cancer Res.* **17**, 4400–4413 (2011).
43. Ivashkiv, L. B. IFNγ: signalling, epigenetics and roles in immunity, metabolism, disease and cancer immunotherapy. *Nat. Rev. Immunol.* **18**, 545–558 (2018).
44. Krishnan, N. et al. A modular approach to enhancing cell membrane-coated nanoparticle functionality using genetic engineering. *Nat. Nanotechnol.* **19**, 345–353 (2024).
45. Wilson, J. T. et al. pH-Responsive nanoparticle vaccines for dual-delivery of antigens and immunostimulatory oligonucleotides. *ACS Nano* **7**, 3912–3925 (2013).
46. Wang, C. et al. Manganese increases the sensitivity of the cGAS-STING pathway for double-stranded DNA and is required for the host defense against DNA viruses. *Immunity* **48**, 675–687.e677 (2018).
47. Kreiter, S. et al. Mutant MHC class II epitopes drive therapeutic immune responses to cancer. *Nature* **520**, 692–696 (2015).
48. Hos, B. J. et al. Identification of a neo-epitope dominating endogenous CD8 T cell responses to MC-38 colorectal cancer. *Oncoimmunology* **9**, 1673125 (2019).
49. Efremova, M. et al. Targeting immune checkpoints potentiates immunoediting and changes the dynamics of tumor evolution. *Nat. Commun.* **9**, 32 (2018).
50. González, F. E. et al. Tumor cell lysates as immunogenic sources for cancer vaccine design. *Hum. Vaccin Immunother.* **10**, 3261–3269 (2014).
51. Engelhard, V. H. Structure of peptides associated with class I and class II MHC molecules. *Annu Rev. Immunol.* **12**, 181–207 (1994).
52. Bassani-Sternberg, M., Pletscher-Frankild, S., Jensen, L. J. & Mann, M. Mass spectrometry of human leukocyte antigen class I peptidomes reveals strong effects of protein abundance and turnover on antigen presentation. *Mol. Cell Proteom.* **14**, 658–673 (2015).
53. MacNabb, B. W. et al. Dendritic cells can prime anti-tumor CD8(+) T cell responses through major histocompatibility complex cross-dressing. *Immunity* **55**, 982–997.e988 (2022).
54. Zeng, F. & Morelli, A. E. Extracellular vesicle-mediated MHC cross-dressing in immune homeostasis, transplantation, infectious diseases, and cancer. *Semin. Immunopathol.* **40**, 477–490 (2018).
55. Li, Y. et al. CD47 cross-dressing by extracellular vesicles expressing CD47 inhibits phagocytosis without transmitting cell death signals. *eLife* **11**, e73677 (2022).
56. Ellis, J. M. et al. Frequencies of HLA-A2 alleles in five U.S. population groups. Predominance Of A*02011 and identification of HLA-A*0231. *Hum. Immunol.* **61**, 334–340 (2000).

57. Chen, K. Y., Liu, J. & Ren, E. C. Structural and functional distinctiveness of HLA-A2 allelic variants. *Immunol. Res.* **53**, 182–190 (2012).
58. Nagao, M. et al. The impact of interferon gamma receptor expression on the mechanism of escape from host immune surveillance in hepatocellular carcinoma. *Hepatology* **32**, 491–500 (2000).
59. Li, L. et al. Cross-dressed CD8α+/CD103+ dendritic cells prime CD8+ T cells following vaccination. *Proc. Natl. Acad. Sci. USA* **109**, 12716–12721 (2012).
60. Reich, Z. et al. Stability of empty and peptide-loaded class II major histocompatibility complex molecules at neutral and endosomal pH: comparison to class I proteins. *Proc. Natl. Acad. Sci. USA* **94**, 2495–2500 (1997).
61. Delamarre, L., Pack, M., Chang, H., Mellman, I. & Trombetta, E. S. Differential lysosomal proteolysis in antigen-presenting cells determines antigen fate. *Science* **307**, 1630–1634 (2005).
62. Savina, A. et al. NOX2 controls phagosomal pH to regulate antigen processing during crosspresentation by dendritic cells. *Cell* **126**, 205–218 (2006).
63. Savina, A. et al. The small GTPase Rac2 controls phagosomal alkalinization and antigen crosspresentation selectively in CD8(+) dendritic cells. *Immunity* **30**, 544–555 (2009).
64. Duong, E. et al. Type I interferon activates MHC class I-dressed CD11b(+) conventional dendritic cells to promote protective anti-tumor CD8(+) T cell immunity. *Immunity* **55**, 308–323.e309 (2022).
65. Elewaut, A. et al. Cancer cells impair monocyte-mediated T cell stimulation to evade immunity. *Nature* **637**, 716–725 (2024).
66. Smyth, L. A. et al. The relative efficiency of acquisition of MHC:peptide complexes and cross-presentation depends on dendritic cell type. *J. Immunol.* **181**, 3212–3220 (2008).
67. Liu, C. et al. A nanovaccine for antigen self-presentation and immunosuppression reversal as a personalized cancer immunotherapy strategy. *Nat. Nanotechnol.* **17**, 531–540 (2022).
68. Murata, S. et al. Regulation of CD8+ T cell development by thymus-specific proteasomes. *Science* **316**, 1349–1353 (2007).
69. Purcell, A. W., Ramarathinam, S. H. & Ternette, N. Mass spectrometry–based identification of MHC-bound peptides for immunopeptidomics. *Nat. Protoc.* **14**, 1687–1707 (2019).
70. Huber, F. et al. A comprehensive proteogenomic pipeline for neoantigen discovery to advance personalized cancer immunotherapy. *Nat. Biotechnol.* 1–13 https://doi.org/10.1038/s41587-024-02420-y (2024).
71. Hoenisch Gravel, N. et al. TOFIMS mass spectrometry-based immunopeptidomics refines tumor antigen identification. *Nat. Commun.* **14**, 7472 (2023).
72. Abelin, J. G. et al. Mass spectrometry profiling of HLA-associated peptidomes in mono-allelic cells enables more accurate epitope prediction. *Immunity* **46**, 315–326 (2017).
73. Wang, C. et al. CD300ld on neutrophils is required for tumour-driven immune suppression. *Nature* **621**, 830–839 (2023).

Acknowledgements

OT-1 TCR transgenic mice and *B2m*$^{-/-}$ mice were kindly provided by Jianhua Li at Key Laboratory of Medical Molecular Virology, Shanghai Medical College of Fudan University. We thank Xiaofang Li and Xiaoyi Jiang at Fudan University, Yiguang Wang at Peking University, Suxin Li at China Pharmaceutical University and Chaoxiong Wang at the Center for Excellence in Molecular Cell Science for technical help and discussion of the paper. This study was funded by the National Natural Science Foundation of China (82341025 and 82272142 to M.L., and 32270137 to Z.L.) and the National Key Research and Development Program of China 2023YFC2706301 (M.L.).

Author contributions

M.L. and Z.L. conceived the project. Y.L., M.F., and H.Y. performed screen experiments and analysis. Y.L. with the help from X.Wei., Z.H., and S.R. performed characterisation of nanovaccine. Y.L. and M.F. performed OT-I stimulation experiments. Y.L. with the help from H.Y. and X.Wang. performed tumour model and analyzed tumour microenvironment. Y.L. with the help from S.X. and Z.J. performed in vitro cell experiments. M.L., Z.L., and Y.L. wrote the manuscript.

Competing interests

The authors declare no competing interests.

Additional information

Supplementary information The online version contains supplementary material available at https://doi.org/10.1038/s41467-025-59977-8.

Correspondence and requests for materials should be addressed to Min Luo.

Peer review information *Nature Communications* thanks Christopher Schliehe, and the other, anonymous, reviewer(s) for their contribution to the peer review of this work. A peer review file is available.